Mitochondrial Membrane Mimic-Induced Structural Dynamics of Cytochrome *c* as Probed by Vibrational Spectroscopy

A Thesis

Submitted to the Faculty

of

Drexel University

by

Dmitry Malyshka

in partial fulfillment of the

requirements for the degree

of

Master of Science

June 2017

ACKNOWLEDGEMENTS

First and foremost, I would like to thank Reinhard Schweitzer-Stenner, my research advisor, for the support, guidance, and all the talks over the four years that I have been fortunate enough to spend and enjoy in his research group.

I would like to thank the members of the chemistry department at Drexel University, especially those who I have bothered repeatedly in order to use their instruments. This includes members of Dr. Ji's and Dr. Xi's groups for the use of the sonicator and Dr. Foley's group for use of the DLS instrument.

Lastly, I would like to acknowledge all of the past and present members of the Biospectroscopy research group, specifically Leah Pandiscia, Bridget Milorey, and Dave DiGuiseppi for the mentoring, the discussions, and, most of all, the good times that were shared.

TABLE OF CONTENTS

LIST OF TABLES

LIST OF FIGURES

ABSTRACT

Mitochondrial Membrane Mimic-Induced Structural Dynamics of Cytochrome *c* as Probed by Vibrational Spectroscopy

Dmitry Malyshka

Dr. Reinhard Schweitzer-Stenner

Cytochrome *c* has been widely studied as an electron transport protein due to its main function as an electron shuttle in the mitochondria. It performs this role via its native methionine/histidine ligation of the heme group, and ultimately drives ATP formation by indirectly pumping protons across the inner mitochondrial membrane to form a gradient. However, more recently, it was shown that cytochrome *c* plays a rather large part in apoptosis, a role it must play though the gaining of peroxidase activity on the surface of the cardiolipin-containing membrane (inner mitochondrial membrane). How does it balance the two functions? Binding studies have now shown that there are multiple binding sites (A, C, and L). Furthermore, some binding models have been proposed as well that treat the binding as a CL-dependent conformational equilibrium between native-like and non-native like states. However, the question as to what the exact structural configuration of these states is still outstanding, along with the unresolved issue of cardiolipin headgroup ionization. Though infrared spectroscopy experiments, it was shown that CL is doubly ionized at neutral pH, with DFT calculations aimed at aiding in the analysis and assignments of phosphate group infrared specra. With resonance Raman, a new experimental strategy is introduced where photoreduction can be used to trace the amount of the non-native-like bound state lacking the native methionine ligation. Furthermore, when the binding was measured at the biologically relevant slightly acidic pH, distinct evidence for the presence of high-spin was observed. Clearly, these states are the prime

candidates for peroxidase activity. Furthermore, the different mode of binding observed at slightly acidic pH is most likely due to the protonation of one of the histidine residues that is responsible for replacing the native methionine during CL-induced unfolding.

(page intentionally left blank)

CHAPTER 1 - INTRODUCTION

1.0 - Protein Folding/Unfolding and Its Relation to Function

The many levels of protein structure and their influences on the biochemical function have been the subject of numerous studies over the past century. For a long time researchers believed that a protein must adopt a very precise conformation in order to be able to carry out its biological function, and this precise structure-function relationship has served as background for many biochemical models, with the outdated lock-and-key model of enzyme-substrate binding as an example. Recently, however, such a narrow view of the structure-function relationship has come under increasing scrutiny with the discovery of numerous vital functions performed by intrinsically disordered proteins in living cells.[1-2] Clearly, proteins that are partially unfolded or have no distinct regular structure at all are capable of functioning properly.

Studies reported in this thesis have focused on one protein in particular, cytochrome *c*, that was found to be able to perform a function even after losing parts of its native tertiary structure. In its native state in the mitochondria, cytochrome *c* acts as an electron carrier between Complex III and Complex IV of the electron transport chain during cellular respiration; a role it can perform via oxidation/reduction of the iron atom of its heme group. Recently, however, cytochrome *c* has been implicated as a pro-apoptotic trigger, a role it performs through a series of complicated biochemical steps. One of these steps involves it acting as a peroxidase; a function many believe it must perform in a partially unfolded conformation in order to facilitate the access of H_2O_2 and the substrate to the heme iron. The extent to which the protein must unfold is currently unclear, and this subject has drawn

the current interest of many researchers. These studies have focused on characterizing the interactions and conformational transitions that are responsible for allowing this protein to perform two completely different and mutually exclusive functions. This thesis describes experiments aimed at identifying sub-ensembles of native-like and partially unfolded oxidized cytochrome c on the surface of anionic liposomes by utilizing resonance Raman spectroscopy.

Moreover, cytochrome *c* has been implicated in other biochemical processes such as acting as a reactive oxygen species scavenger as well as having a role in the self-aggregation of α-synuclein in Parkinson's disease.[3-4] The extent of these functions in the living organism is still not clear. They will not be considered further in this thesis.

This introductory chapter proceeds with a description of the driving forces of folding and unfolding, which includes solvent-protein as well as membrane-protein interactions. This will be followed by a discussion of the process of folding/unfolding itself. The third sub-chapter is a description of how these forces and studies apply to proteins in general before focusing in on the native structure and function of cytochrome *c* and those of its partially unfolded conformations, with particular focus on previous studies that have utilized vibrational spectroscopy to study cytochrome *c* and its conformational equilibria.

Ultimately, after providing a well-rounded account of the history of research on cytochrome *c* and its conformational transitions, this thesis presents a vibrational spectroscopy approach of studying the structural equilibria of cytochrome *c* on the surface of anionic lipid membranes. Along the way, the results presented are discussed in the context of the existing literature.

1.1 - Overview of Protein Folding and Unfolding

While nucleic acids, carbohydrates, and fatty acids all have many important functions in the organism, it is quite clear that proteins are responsible for the majority of biochemical processes and functions. Be it enzymes driving important reactions or proteins serving as structural building blocks of cellular macrostructure or as transport proteins, organisms rely heavily on proteins performing their functions extremely well. It has been obvious from the very beginning that even a single protein that cannot perform its function can have widespread effects on the organism, with a popular example being sickle-cell anemia, where a single amino-acid residue difference allows hemoglobin to polymerize when little oxygen is present and disrupt its function. Another example is the aggregation and large-scale fibrilization of misfolded amyloid β (Aβ) peptides subunits and Tau proteins, processes both involved in Alzheimer's disease. It is clear that protein misfolding can have highly degenerative effects, but to properly study such diseases one must understand in detail what drives protein folding and unfolding.

There are four levels of protein structure. The sequence of the protein's amino acids, i.e. the building blocks of peptides, is the protein's primary structure.[5] However, the primary structure is one dimensional, simply a "list" of the arrangement of the twenty possible amino acids in the sequence that can be thousands of amino acids long. These amino acids, consisting of a carboxyl group, amino group, and a variable R group on the center carbon, polymerized through peptide bonds providing the protein with a simple repeating "backbone" of C-C-N. It is the identity of the R groups that allows the individual amino acids and ultimately the protein to interact individually with their surroundings. For example, aliphatic side chains on amino acids such as isoleucine (isopropyl R group) or

phenylalanine (a benzyl R group) would avoid an aqueous solvent while preferring each other, whereas polar or charged amino acids such as serine (methanol as the R group) and histidine (imidazole R group) are expected to interact favorably with an aqueous solvent. The combination of these interactions on the local scale drives the formation of structures like α-helices and β-strands, i.e. the protein's secondary structure. Concurrently, the entire protein structure rearranges into its tertiary structure, which together with the secondary structure identifies the final folded state of the protein. An example of quaternary structure is multiple separate subunits coming together into a single macrostructure, with a classical example being hemoglobin composed of two α and two β subunits.[6] While the latter three-dimensional structures can be altered e.g. by addition of denaturing agents or altering of the temperature, the protein's primary structure can only be altered through cleavage of peptide bonds, a function generally done by specific enzymes called proteases, or via mutagenesis.

It became clear in the 1960's after Alfred Anfinsen's experiments with ribonuclease A that primary structure ultimately guided the final protein shape.[7] In his experiments, Anfinsen unfolded ribonuclease A by first reducing the disulfide bridges via mercaptoethanol and following it with the addition of urea. After removal of these denaturants the protein refolded back into its native form, showing that protein folding was encoded in the primary structure of the protein rather than being a result of external influences. However, what exactly drives protein folding? It is clearly not random sampling of possible conformations, as the free rotation of the protein backbone allows for a virtually infinite number of possibilities that would take an impractically long time to sample, even for relatively short peptides. Rather than random sampling, Levinthal suggested that proteins follow a

sequential energy pathway that is guided by local interactions, as has been described above, which allow the protein to ultimately obtain a conformation that is at an absolute Gibbs free energy minimum.[8] These local interactions can include hydrogen bonding, electrostatic interactions, or hydrophobic interactions, the latter of which has even been proposed by Kauzmann to be the major driving force behind protein folding as far back as 1959 mainly due to the large entropic stabilization of the protein structure.[9]

This view was essentially confirmed, though a bit modified, by the 1990's after decades of studies on protein folding. By this time, it was clear that it was indeed a combination of multiple driving forces, such as hydrogen bonding, hydrophobic and electrostatic interactions, and possible covalent interactions, that guide the protein folding by minimizing the Gibbs free energy while also minimizing the conformational entropy of the system. While minimizing conformational entropy might not seem as particularly favorable, it gets balanced out by the entropic contribution from the hydrophobic effect as well enthalpic stabilizations from the favorable interactions such as hydrogen bonding. This stabilization was interpreted in the form of a free energy landscape in a shape of a funnel, with multiple local minima associated with the many unfolded or partially-unfolded states and a global minimum representing the native, folded conformation.[10] According to this 'funnel model,' the folding process begins at the "top" of this funnel, moving down as favorable interactions lead to a decrease in free energy. The funnel is rugged due to the many local minima, as shown in Figure 1.1.1. The protein undergoing the folding process can sample many of these minima, which thus represent kinetic intermediates of the folding process. Misfolded states of a protein can also be described as the protein being trapped in one of these local minima, without being able to overcome the energy barrier separating

them from the absolute minimum on the normal time scale of folding processes (10^{-3}-1 s). Such a metastable, even more long living misfolded state was shown to exist for cytochrome *c* by Soffer et al.,[11] where the protein is trapped in a non-native state even at native conditions after it was exposed to alkaline pH.

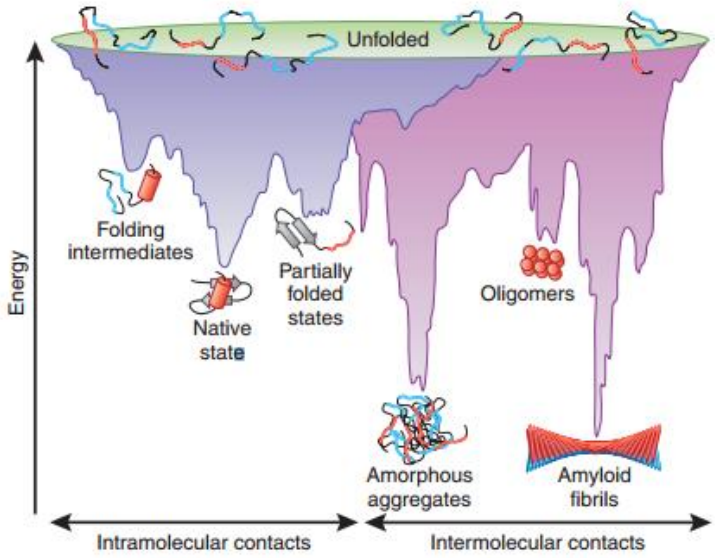

Figure 1.1.1 – Depiction of the rugged funnel model of protein folding, shown here for fibrils.[12]

1.2 – INFLUENCES ON PROTEIN STRUCTURE

It has long been known that protein structure can be altered in quite a few different ways, such as temperature, pH of the solution, or by changing the solvent. With most proteins existing in aqueous environments, unfolding is expected if the solution composition becomes even slightly less polar. Increased temperature is known to denature proteins, mainly due to the breaking of such favorable interactions such as hydrogen bonding (i.e. the protein is provided with energy to escape the global minimum on the free energy

landscape). Cold temperatures have also been known to disable normal functions of enzymes, mainly by making them too "stiff" and unable to act as proper catalysts.[13] pH influences the charges on the ionizable side chains on the protein, dictating which residues will become charged, and thus hydrophilic, or neutral, and thus more hydrophobic. pH related changes to protein structure were quite relevant to past cytochrome *c* studies, as the pH related structural changes have been very well characterized and documented by many scientists over the years. However, there are other possible processes that affect protein structure that are less prominent but important nonetheless. The structure of cytochrome *c* can be changed by its binding to surfaces, which includes cellular membranes, monolayers, and metal surfaces, as will be detailed later.

1.2.1 - *Structure of Cellular Membranes*

Cellular membranes are composed mainly of phospholipids; molecules that are known for being amphiphilic owing due to the long hydrophobic acyl tails and charged hydrophilic headgroups (usually a modified phosphate) bonded together via a glycerol backbone. Thus, phospholipids in aqueous solutions usually form bilayers, with two sheets of phospholipids coming together by letting the hydrophobic tails interact with each other to form a hydrophobic core while exposing the headgroups to the solvent. When the cross-sectional area of a lipid's headgroup is disproportionate relative to the cross-sectional area of its acyl tails, membrane curvature can form. Positive curvature can lead to small spherical aggregates known as micelles,[14] whereas negative curvature can lead to the inverted hexagonal phase.[15] Examples of both types of curvature are shown in Figure 1.2.1. When

the two cross-sectional areas are in proportion, the lipids can form bilayers, including cellular membranes and vesicles (including liposomes, though the degree of curvature depends on liposome size).

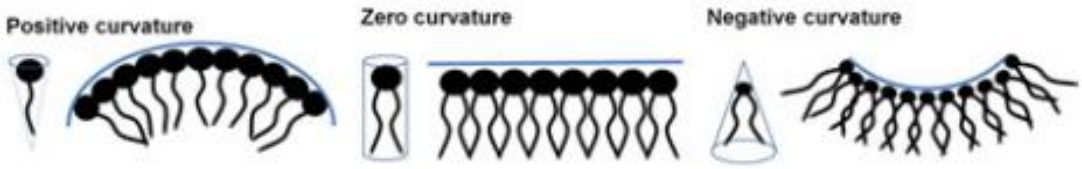

Figure 1.2.1 – Effects of cross-sectional area proportionality between the headgroup and the acyl tails.[16]

The structure of membranes is not necessarily completely fluid, as was initially proposed in the fluid mosaic model by Singer and Nicolson back in 1974.[17] Their model was based on labeling experiments that showed that proteins diffuse through the membrane rather freely at rates dependent on the fluidity of the membrane, and described the lipid components as being able to do the same thing in random fashion. However, more recent experiments have shown that external (proteins, ligands, etc.) and internal (composition of the membrane) forces play a rather large role in determining the structure of the membrane. It is clear that many physical properties of the membrane are directly dependent on the identity of both lipids and other possible components of the membrane and its surface, such as proteins, carbohydrates, and cholesterol. Some experiments have shown that lipids can demix to form co-operative "rafts" upon interacting with proteins, a phenomenon that cannot be described as random.[18] Hartmann and Galla's experiments in 1978 with polylysine showed that the binding of the peptide to the membrane surface not only induced a conformational change in the peptide but also led to a curvature of the membrane.[19]

1.2.2 – Membrane Induced Conformational Transitions

Membrane-induced conformational transitions include both folding and unfolding. An example of the former is α-synuclein, an intrinsically disordered protein 140 residues long that has been implicated to play a heavy role in Parkinson's disease. In solution, this protein can be considered as unfolded.[20] However, numerous studies have pointed to it adopting a variety of conformations when binding to different surfaces. For example, NMR studies have suggested that a part of the protein adopts an α-helical configuration upon binding to sodium dodecyl sulfate micelles.[21] Furthermore, it is the protein's ability to form β-rich aggregates that defines its detrimental role in Parkinson's disease,[22] clearly showing that membranes can induce protein folding. An example of unfolding on the membrane surface is a myosin-type protein called myosin VI, an intracellular molecular transport protein. Myosin VI is classified as a relatively short myosin family protein, but was found to take surprisingly large "steps" in the cell. It was found that the protein can bind to a membrane and unfold, in the process becoming longer and actually capable of taking the abnormally large steps.[23] Another prominent example of membrane-induced unfolding is cytochrome *c*, the focus of this thesis, which will be followed up below.

1.3 – Cytochrome *c*

1.3.1 - Structure and Function of Native Cytochrome c

Cytochrome *c* is a relatively small protein of 104 amino acid residues, with small variations between species, with an example shown in Figure 1.3.1. Among its highly conserved structures are the two main α-helical units, termed the N- and C-helices that interact together and stabilize the protein.[24] They are stable enough to be the last units to unfold (more on the foldon model below). Aside from another short helix, the protein mainly consists of loop structures. Another important conserved structural unit is the heme group (also shown in Figure 1.3.1), i.e. an iron porphyrin, that is anchored to two cysteine residues of the protein (C14 and C17) through thioether linkages, and two axial ligands, a histidine (H18) and methionine (M80).[24-25] Furthermore, there is a presence of a conserved water molecule (termed Wat166) on the interior of the protein that, along with an arginine (N52) and a tyrosine (Y67), forms an internal hydrogen bonding network.[26] The two ligands along with the four nitrogen atoms of the porphyrin ring produce a low spin configuration of the central iron atom. The redox potential of the protein of ~0.2 V[27] favors the reduced (ferro-) state. The M80 ligation is pivotal for maintaining this redox potential.

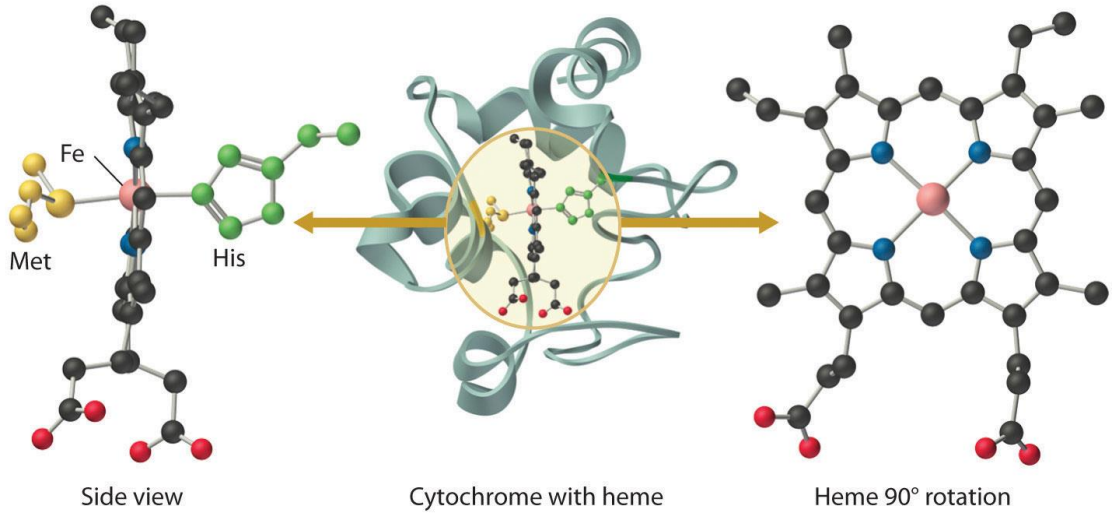

Figure 1.3.1 – Structure of cytochrome *c*, with emphasis on the heme group and its native histidine/methionine ligation state.[28]

Cytochrome *c* possesses 19 lysine residues, which gives the protein its high isoelectric point of approximately 10.5 and a +8 charge at neutral pH. This allows cytochrome to interact with negative surfaces and molecules, and it also imposes a high sensitivity to ionic strength. UV/Visible absorption experiments by Shah and Schweitzer-Stenner showed that the protein adopts a more compact state in the presence of hypophosphite anions (and acetate anions, to a lesser extent), where they observed an increase in oscillator strength for the charge transfer band at 695 nm that indicates a strengthening of the iron-M80 linkage.[29] These results are supported by separate small angle X-ray scattering[30] and UV resonance Raman experiments.[31]

The heme group itself has been introduced above as the main functional unit of the protein. In the native state, it is buried in a hydrophobic pocket of the protein. Thus it is mostly protected from the solvent with only a corner exposed.[32] While a free heme group is planar with its macrocycle exhibiting approximately D_{4h} symmetry due to aromaticity and a hexacoordinate geometry, the complex protein structure around it causes symmetry-lowering deformations.[33] Shelnutt and co-workers studied many species of cytochrome c to show that many aromatic and charged residues near the heme pocket have structural influences on the heme, and that the conserved thioether linkages induce the ruffling of the heme group.[34] Ruffling is one of many possible out-of-plane deformations observed in heme groups, with doming in hemoglobin and myoglobin being examples. Ultimately, these deformations and the structural elements that cause them govern the functional ability of the protein. For example, the non-planarity of the heme group and the identity of the

ligands function to define the protein's redox potential and thus its ability to function as an electron carrier, with Liptak et al. showing that the ruffling distortion destabilizes the iron's *d*-orbitals and lowers the redox potential.[35] The protein environment also imposes chirality onto the heme group, leading to a pronounced circular dichroism signal that has been used widely to study this protein.

The native protein can adopt +2 and +3 oxidation states of its heme iron that allow it to function as an electron carrier. While most of the studies in this thesis will focus on the +3 oxidation state, it should be mentioned that ferrocytochrome *c* only has minor structural differences from its oxidized counterpart.[36] There is an overall weakening of the Fe – M80 ligation,[37] and an overall stabilization of the protein is observed. The reduced state is stable up to much higher temperatures as well as more extreme pH values.

In its native form, the protein functions as an electron carrier from Complex III to Complex IV, as shown in Figure 1.3.2. The process of reduction at Complex III and the subsequent oxidation at Complex IV drives the transport of protons from the matrix into the intermembrane space. This proton pumping creates a slightly alkaline matrix (pH ~8), while the pH of the intermembrane space is slightly acidic (pH ~6.9).[38] This, in turn, creates a proton as well as an electric gradient, both of which drive the formation of adenosine triphosphate (ATP), the cell's "energy currency," at the IMM's ATP synthase. Disruption of regular cytochrome *c* function would thus halt cellular respiration by effectively "overloading" Complex III with electrons, which in turn would start to produce reactive oxygen species (ROS). Such species can cause damage inside the mitochondria and the cell, highlighting the importance of proper cytochrome *c* function. Its native function is highly dependent on the protein remaining in its native conformation, as the loss of the

M80 ligation results in an approximately 500 mV drop in redox potential from ~0.2 V to ~ -0.3 V.[39] This puts it outside the range of catalysis by Complex III.

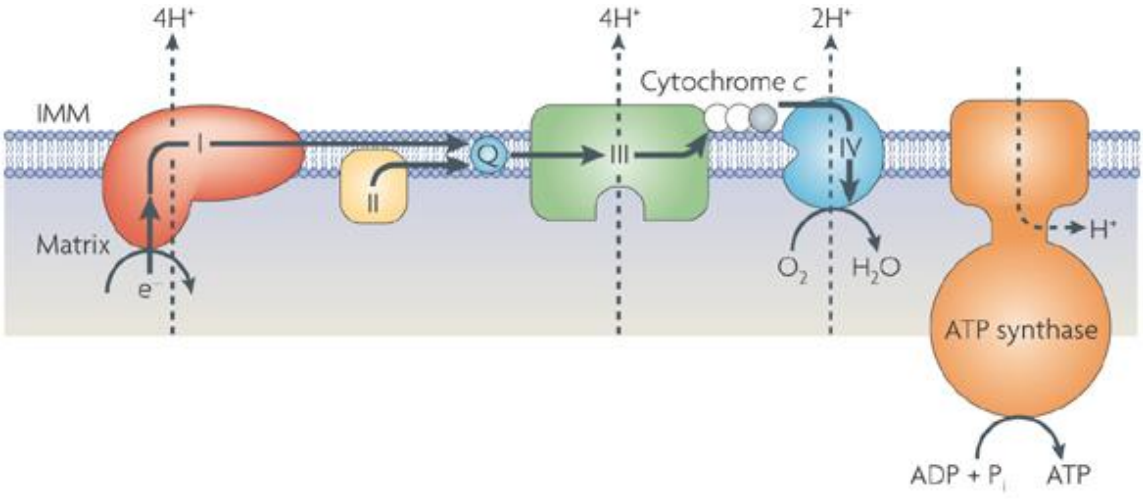

Figure 1.3.2 – Role of native cytochrome *c* on the surface of the mitochondria, where it functions as an electron carrier that ultimately drives ATP synthesis.[40]

It is clear that conformational transitions inhibit cytochrome *c*'s regular function. This thesis explores cardiolipin-induced conformational transitions and their possible role in the protein's role in apoptosis. In order to understand them, however, it is important to understand the previously described conformational equilibria of cytochrome *c* in solution.

1.3.2 - *pH Dependent Conformational Changes*

Due to the presence of many charged residues on the surface of the protein (pI of ~10.5) as described earlier, it is not a surprise to learn that cytochrome *c* is sensitive to pH changes. Theorell and Åkesson were the first to elucidate such changes with equine cytochrome *c* via classical pH titration studies in 1941.[41] Further studies since then aimed at the structural

characterization of these states via multiple spectrophotometric techniques yielded a clearer picture. With the addition of acid, the protein keeps its native state (H18/M80 ligation) all the way down to a pH of approximately 4.5, where it switches to any of a variety of possible conformations. Of these, the dominant conformer is a low-spin bis-His species (H18/H33) with small contributions from a high-spin water-ligated species (H18/H_2O) and possible high-spin pentacoordinated species (H18/-).[42-45] Decreasing the pH results in a transition at a pH of approximately 2, where the protein adopts an unfolded conformation.[46] This conformer shows ionic strength dependent behavior, where it moves away from a statistical coil to a more molten globule-like state with increasing ionic strength.[46] When moving from neutral to alkaline pH the protein remains at its native conformation up to a pH of ~8.0, where it exhibits a transition into any of many coexisting states (which are dependent on the species of cytochrome *c*). In the equine protein, there is a co-existence of three low-spin sub-conformers defined by the replacement of the M80 ligation with one of three possible lysine residues (K72, L73, K79), and this replacement is termed the "alkaline transition" of the protein.[47] Above pH 11, the protein undergoes further changes, replacing the lysine ligation with a water molecule or a hydroxide anion.[48] Per Theorell and Åkesson's titration starting at a pH of 1.5, these states were numbered I-V starting from the acidic conformer below the pH of 2. This is exhibited by Figure 1.3.3.

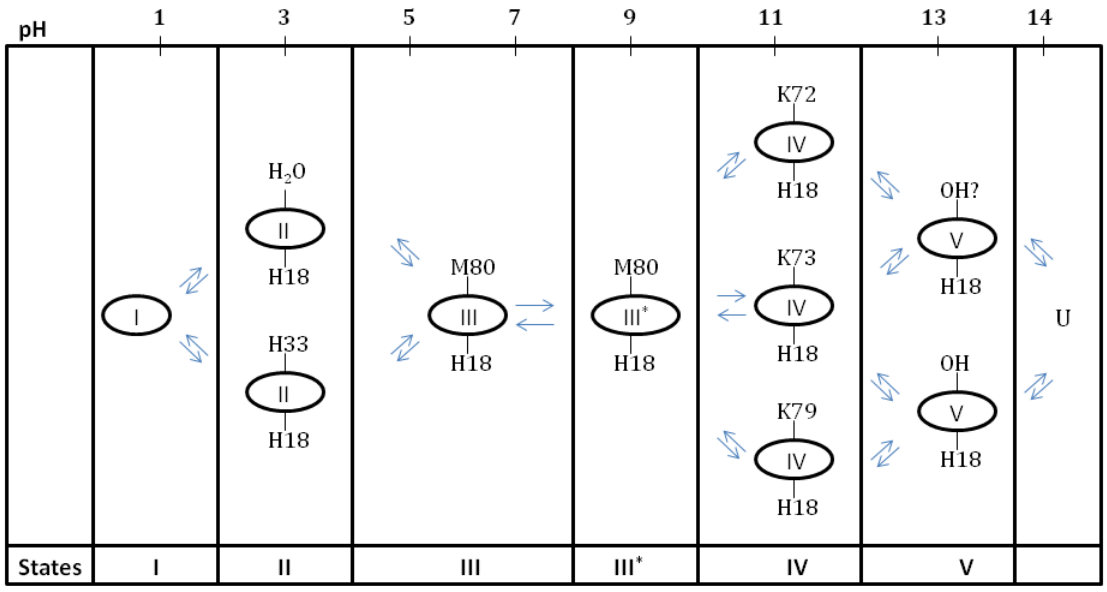

Figure 1.3.3 – pH dependent conformational transitions of cytochrome *c*, with all six conformational states described in the text labeled I – V.[49]

Through more recent experiments, additional conformations were discovered. At neutral pH, a kinetic bis-His intermediate was discovered when the protein was allowed to refold after being unfolded via guanidine chloride.[50] This state was originally detected in the completely unfolded protein, but its exact ligation was also observed transiently during the refolding process. Another thermodynamic intermediate was found at slightly alkaline conditions and low ionic strength by Verbaro et al., where an overall weakening (but not a complete loss) of the M80 ligation was detected.[51] This state came to be termed State III* (reflected in Figure 1.3.3). It was assigned to the deprotonation of one of the propionic acid residues on the heme group itself by Bowler and coworkers.[52] Experiments at high ionic strengths by Romesberg and coworkers revealed another state in the same pH region, termed 3.5, that preceded the alkaline transition.[53] State 3.5 was characterized by a complete loss of the M80 ligation to the protein, contrary to what was observed for the III*

state. Furthermore, work by Soffer et al. showed the existence of a misfolded conformer at neutral pH that was achieved by quickly allowing the protein to refold after keeping it in State V for 1 week.[11] This state was attributed to a stabilized hydroxyl-ligated V state.

1.3.3 – Foldon Model

As described above, the folding process can encompass multiple folding intermediates that only exist transiently (<1s timescale), making it highly difficult to achieve any structural characterization. Hydrogen-deuterium exchange (HX) rates can be measured via proton-NMR and provide residue specific information, where exchange rates are expected to be high for residues exposed to the solvent and low for residues buried in the protein. Englander and coworkers utilized this method for cytochrome *c* at low denaturant concentrations to observe multiple such intermediates for cytochrome *c* in the process of re- or unfolding that they attributed to different folding units, termed foldons.[54] These foldons behaved as single units that folded seemingly independently from each other, characterized by different free energies of folding.[55] These are reflected in Figure 1.3.4. The loop containing the M80 ligation, red in the figure, is the easiest to unfold and is thus the most unstable. The yellow foldon in the figure is the second to unfold, followed by green foldon and then the blue foldon. The unfolding of the yellow foldon leads to the exposure of the heme group to the solvent. The green foldon contains the 60's helix, while the very stable C- and N-terminal helices are the blue foldon.

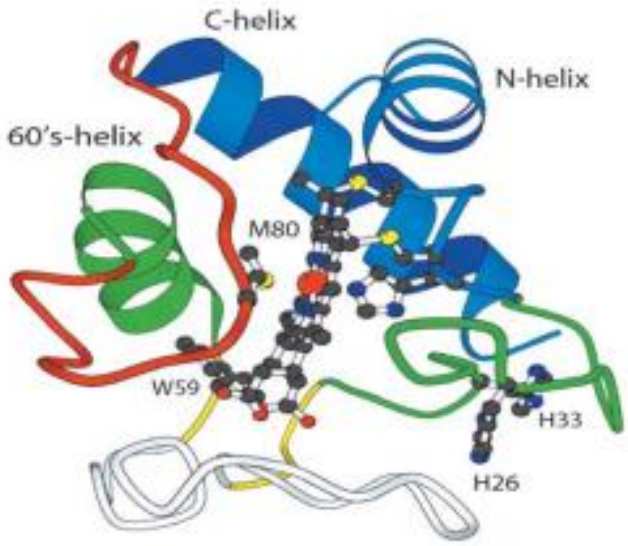

Figure 1.3.4 – Structure of cytochrome *c*, with different foldon units of the protein clearly labeled.[55]

1.3.4 – Alternate Function: Apoptosis and the Importance of Cardiolipin

By the early 1980's, the work of de Kruijff and co-workers had established the peculiar interaction between cytochrome *c* and CL.[14] By the late-1990's, it had been shown that cytochrome *c* could undergo conformational transitions upon binding to the inner mitochondrial membrane and that these conformational changes were the driving force behind the protein's newly acquired peroxidase activity, which in turn catalyze the peroxidation of mitochondrial lipids and cytochrome's release from the mitochondria – all steps being a requirement for cytochrome's role in apoptosis.[56] There is no question that proper control of apoptosis is vital due to its role in cancer and auto-immune diseases, among other important roles in normal development and organism homeostasis. Cytochrome *c*'s biochemical role in this process has been since mapped out, though some

of the details as to how it leaves the mitochondria to trigger the apoptotic cascade are still unclear.

Upon being released from the mitochondria, the protein binds to the apoptoptic protease activating factor 1 (APAF1) to form a quaternary structure called an apoptosome. The apoptosome can then bind to pro-caspase-9 to activate it, and activated caspase-9 goes on to activate more caspases which are responsible for executing apoptosis.[57] This process is depicted in detail in Figure 1.3.5. None of the steps following the release of cytochrome *c* can be stopped, effectively committing the cell to death. For this, the release of cytochrome *c* from the mitochondria is sometimes referred to as the "point of no return" in apoptosis. It should be noted that to trigger cytochrome *c* release, the cell must have initiated an apoptotic trigger cascade that has multiple checkpoints and that cytochrome's release is thus far from being the first apoptotic step.

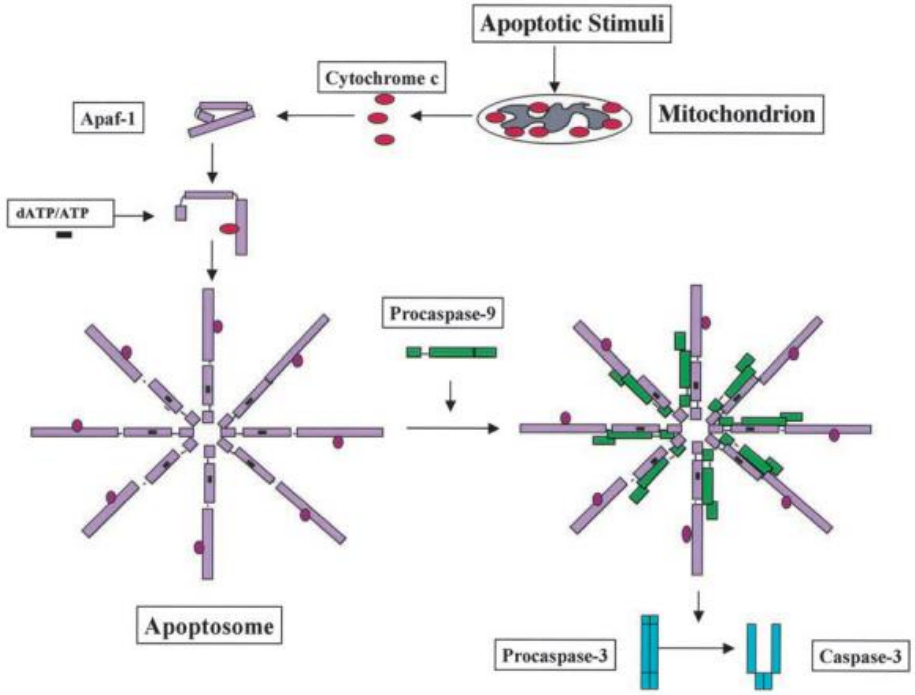

Figure 1.3.5 – Formation of the apoptosome by release of cytochrome *c* into the cytosol.[57]

The marked change in function from electron carrier to peroxidase is triggered by the protein's interaction with cardiolipin (CL),[58] a unique phospholipid generally found on the inner mitochondrial membrane and in some bacteria whose structure is shown in Figure 1.3.6.

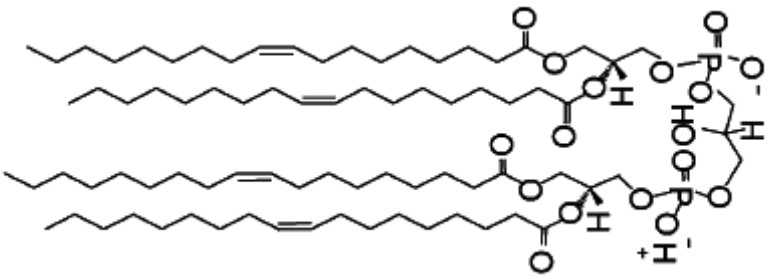

Figure 1.3.6 – Structure of a variant of cardiolipin called tetraoleylcardiolipin.

CL is unique because it has two phosphate headgroups and four acyl chains as compared to the one phosphate / two acyl chains structure of most phospholipids. In essence, the structure is simply two phosphatidic acid residues connected together via their headgroups through glycerol. The two phosphate headgroups can provide CL with a -2 charge, but the biological ionization state of CL has been under debate. A commonly accepted model by Kates et al. assigns pK_a values of 2.8 and ~8.5 to the two phosphate headgroups based on a proposed "proton trap" through a bicyclic resonance stabilization of monoionized CL.[59] These results were indirectly supported by Lemmin et al.'s molecular dynamics simulations, where the authors were able to explain some properties of CL-rich membranes by having a monoprotonated CL molecule.[60] Kates model was directly supported by *ab initio* calculations, which showed the presence of the proposed bicyclic structures.[60] However, these results are at variance with some older studies[61-62] as well as some recent titration experiments[63] that all point at a dibasic view of the molecule. The primary mode of interaction between cytochrome *c* and CL is expected to be electrostatic – thus, for

proper interpretation and understanding of the binding, the exact protonation state of CL must be known. One part of this thesis focuses on resolving this issue.

CL composes approximately 20 mol% of all mitochondrial lipids, with the majority (~80%) of CL residing in the inner leaflet of the IMM.[58] Under normal cellular operation, approximately 15% of the CL in the outer leaflet of the IMM is bound to cytochrome *c*,[64] allowing the protein to be loosely associated with the membrane and the electron transport chain. However, apoptotic signals cause a rapid flux of CL molecules from the inner leaflet to the outer leaflet as well as the inner leaflet of the outer mitochondrial membrane. Ott et al. have proposed a mechanism where the cytochrome first solubilizes in the intermembrane space and causes the Bax and Bak proteins to become active. These proteins then promote the formation of MAC, which provides cytochrome a direct route out of the mitochondria.[65] This process is shown in a simplified diagram in Figure 1.3.7.

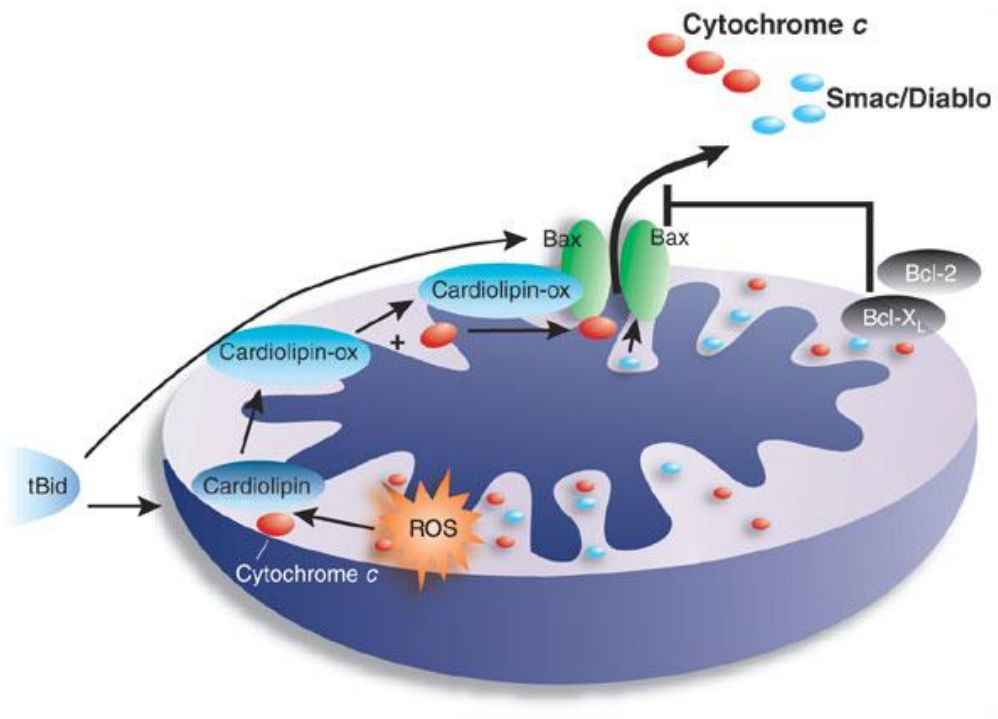

Figure 1.3.7 – The biochemical pathway cytochrome *c* experiences in order to trigger apoptosis.[66]

The mechanism of release of cytochrome *c* from the membrane, however, is not entirely clear. It has been shown that cytochrome *c* gains peroxidase activity during this process, and that it must do so to perform its pro-apoptotic function.[67-69] However, cytochrome *c* is quite different from classical peroxidases in that it does not allow an easy access to the active site. Classic peroxidases such as horseradish peroxidase contain a heme group, as well, but the heme is pentacoordinated to allow access to H_2O_2, with a water molecule near the proximal site forming a hydrogen bonding network with an arginine and a histidine residue that together stabilize the ferryl state of compound I.[70] Furthermore, the mechanism of peroxidation and the intermediates (compound I and compound II) involved have been described and detected, even if transiently, for classical peroxidases.[71-73] Not only is the native structure of cytochrome *c* not particularly amenable to peroxidase activity, there has

also been no direct evidence for the presence of compound I and compound II intermediates as of yet. Though some measurable peroxidase activity is present with State III cytochrome *c* (a second-order rate constant of ~10^4 M^{-1} s^{-1}), it performs this function much slower than horseradish peroxidase (~10^6 M^{-1} s^{-1}).[71] McClelland et al. showed that the cytochrome mutation K72A enhances peroxidase activity by possibly destabilizing the loop containing M80.[74] This highlights the role of the Fe-M80 ligation in modulating the peroxidase activity. It is very weak even for native cytochrome *c*, and its rupture is one of the first conformational changes that cytochrome exhibits upon interacting with CL. Such a change not only overcomes the main kinetic barrier for cytochrome *c*'s peroxidase activity but also inhibits the protein's native function, highlighting the delicate balance between CL and cytochrome *c* that the cell must maintain for proper function and to avoid unnecessary peroxidation. It has been shown that cytochrome *c* with the exposed heme group can rapidly gain noticeable peroxidase activity,[75] with the notable exception being state IV. However, what exact structural changes and triggers are responsible for this, and how can the cell balance these two mutually exclusive functions?

1.4 – Resonance Raman and Heme Proteins

Raman spectroscopy is considered a vibrational spectroscopy tool that complements the more common infrared spectroscopy. While infrared (IR) spectroscopy is a rather simple absorption technique, Raman spectroscopy utilizes an inelastic scattering mechanism with a completely different set of selection rules where the Raman activity is dependent on a change in the molecule's polarizability rather than the dipole moment. Differences between

the frequencies of scattered and incident light correspond to the vibrational modes of the studied molecule(s). Due to the difference in selection rules, different types of vibrational modes can be elucidated (e.g. the symmetric stretch of CO_2 is a famous example – it is IR inactive, but Raman active). Resonance Raman (RR) spectroscopy, however, utilizes the electronic excitation of the heme macrocycle to enhance the scattering cross section of its vibrational modes by several orders of magnitude. Detailed explanations will be presented further below. Through a series of works by several groups discussed later in this thesis, it has been shown that the RR spectrum of cytochrome c is highly sensitive to the heme's ligation, spin, oxidation, and conformational states.

1.4.1 – Binding of Cytochrome c to Electrodes Probed via Resonance Raman

Thomas Spiro and his coworkers measured and interpreted the RR spectra and the respective depolarization ratios of cytochrome c and hemoglobin.[76] They also attempted a very general assignment of the Raman modes based on the resonance intensity and their depolarization ratios (which are both dependent on the excitation wavelength).[77] Since then, there has been an extensive amount of work done by Spiro and co-workers on both cytochrome c and other heme analogues,[78-81] highlighting the sensitivity of the so-called higher frequency marker bands to changes in the heme's oxidation, spin, and ligation states. Also, some of the low frequency marker bands' Raman activity depend heavily on the out-of-plane distortions of the heme, with ruffling being the primary such distortion for cytochrome *c*.[80] The extent of these works over a range of 20 years has brought Spiro and his group to culminate in a publication summarizing the assignments of most bands in the

Raman spectrum of native cytochrome c.[82] Based on it, the ligation, oxidation and spin states of the heme are quite easy to infer by inspecting the RR spectrum in the region between 1300 and 1700 cm^{-1}. The Schweitzer-Stenner/Dreybrodt group has used Raman spectroscopy to probe distortions of heme proteins, with cytochrome c being one of them, by observing and analyzing the depolarization ratio dispersion and resonance excitation profiles of prominent marker bands in their RR spectra.[83] Through careful analysis based on quantum mechanical perturbation approaches, information about symmetry-classified heme deformations were obtained. This information has also been utilized in observing pH dependent structural transitions of both ferri- and ferrocytochrome *c* by Schweitzer-Stenner and his co-workers, with the data showing a pH dependence for the ferri- species in the alkaline region (associated with the alkaline transition) with no pH dependence for the ferro- species in the same region.[84]

While the basics of the use of Raman spectroscopy to study the structure of cytochrome c laid out in the seventies, eighties, and early nineties, a growing number of groups have since utilized Raman spectroscopy to probe structural changes of cytochrome c upon binding to surfaces, ranging from electrodes in cyclic voltammetry to lipid membranes to mitochondrial mimics. Electrode potentiometry, along with cyclic voltammetry, are very useful techniques in studying redox reactions, and cytochrome c is known to undergo such a reaction *in vivo* during electron transfer, as has been described above. In such measurements, the protein is bound to different types of membrane-coated electrodes (the different electrodes try to emulate different physiologically relevant lipids), with the electrical potential being slowly changed and the response (current) being measured. However, it is rather difficult to explore the structure of the protein during the different

steps of the measurements by most conventional techniques (UV-CD, IR, etc.). This issue was addressed by surface-enhanced Raman spectroscopy (SERS) which provides a great tool for exploring cytochrome c bound to electrodes, and it provided one of the first insights into the structural changes of cytochrome c upon binding to different types of surfaces. Providing enhancement through plasmon resonance, the heme group's Raman signals are enhanced to an extent that allows even single molecule detection.[85] Using this technique, a large variety of studies was performed to characterize the different oxidation states of cytochrome c while bound to different types of membranes, and they are summarized below.

Hildebrandt and associates have performed multiple studies on this topic in the past.[86-90] Through a study where they simply adsorbed cytochrome c to colloidal silver particles, Hildebrandt and Stockburger observed that cytochrome undergoes an "adsorption-induced partial transition" from a native low-spin state to a high-spin state,[91] usually indicative of an iron ligation state change, by observing the spin marker bands in the high-frequency region. From the study, the authors also observed a thermal equilibrium between the two bound and unbound states, indicating a reversibility of the binding process. Later, this group took the study further by first adsorbing cytochrome to a silver electrode in different salt solutions,[86] and then obtaining the SERS spectra at different potentials and analyzing the spin marker bands. From this study, they found the existence of two states that the simply called I and II. The two states have different redox and spin properties, with state I being the more native-like, low-spin state with the native potential of +0.2 V, and state II being a mixture of a penta-coordinated high-spin (5chs) and a hexa-coordinated low-spin state (6cls) with both showing a negative reduction potential (-0.31V and -0.41V,

respectively, with all values being in reference to the standard calomel electrode). The authors proposed that the protein adsorbing to the negative membrane via its lysine residues is what causes the conformational transitions. With State I, the changes in protein structure were very minor, while the structural changes observed in State II where more pronounced, to the effect of changing the heme ligation state. This conclusion was drawn by comparing the spectral changes of State II in acidic solutions to the spectral changes of cytochrome c in unfolding experiments. It is also noteworthy that the silver electrodes exhibited a net positive charge for all potentials used in this study, specifically drawing the anions out of solution to form a "membrane" of negatively charge anions. Cytochrome c, a protein with a +8 charge, thus exhibits some electrostatic interactions with this "membrane".

In the beginning of the 2000's, Hildebrandt and co-workers resumed their work on electrode-bound cytochrome c, this time working with coated metal membranes.[90-91] In the first study, the electrodes were coated with varying-chain-length self-assembled monolayers (SAMs); the interactions were again shown to be mainly electrostatic. Here, Oellerich and Hildebrandt observed additional states of the electrode-bound protein. They introduced new notation: B1 is the native state, and B2 is the electrostatically influenced state with three substates. They noted that the protein retains a mainly native structure at the surface when there is an excess of protein in solution (this, as will later be seen with negatively charged phospholipids, is representative of a *low* lipid-to-protein (L/P) ratios), and termed this as the B1 state. With a high L/P ratio, i.e. when most if not all of the protein is bound to the surface and no protein is free in solution, a definitive change to the B2 state is observed that can be primarily characterized by an altered heme pocket structure. The three substates of B2 can be characterized further by their spin and coordination states

(6cls, 6chs, and 5chs). The study, overall, is quite elegant and highlights the importance of the understanding of the electric field's contribution to the structural changes of cytochrome c.[88] A second study, published a few years after the first, is very similar to the first in style but with very different SAMs. The pyridyl-terminated SAMs that they used are special in that they could bind to the heme by displacing the native M80 ligand so that the heme became exposed to the membrane. The results are a bit inconclusive biologically (since a direct linkage of the heme to the membrane by ligation is most likely not physiologically relevant), but they do mention an important point: the adsorbed protein shows "redox state dependent coordination equilibrium."[90]

Since metal surfaces, even coated ones, are not very biological systems, the extent of the insights that these experiments could offer into the biological picture might be expected to be quite limited. The next section discusses RR studies of more biologically relevant membranes, at the expense of surface-enhanced effects.

1.4.2 – Binding to Lipid Membranes as Probed by Raman Spectroscopy

The binding of cytochrome c to different membranes offers a very wide spectrum of experiments – the high variety of possible membranes allows the probing of many possible structural changes. Since cytochrome c is a very positively charged protein, these studies often focus on negatively charged membranes and surfaces.

As stated above, the Hildebrandt group has also dipped their foot into this field with the electrode studies from 1989.[87] By adsorbing cytochrome c to *highly* negative anions, the authors saw the stabilization of State II (the non-native state with two substates). Also of

note, they saw a destabilization of the 6cls state of the native reduced species upon binding to negatively charged phosphatidylglycerol (PG) membranes, with the protein forming a mixed spin species (two substates of State II, one being high spin with the other low spin). Overall, the point of the study was to show that the electrode experiments actually show some possible biological relevance.

A year later, Hildebrandt and co-workers published another study, focused on the binding of cytochrome to negatively charged phospholipid vesicles (phosphatidylglycerol, namely DMPG, DOPG, DOPC, and a mixture DOPG/DOPC). Noting severe structural changes in the protein upon binding to such vesicles, the authors still found the presence of state I and the two substates of State II (this study was carried out before the shift in notation), with different spectral characteristics. However, the highlight of this study is in its quantitative nature. By taking preliminary SERS spectra as well as published SERS spectral parameters (frequency, half-width, and intensity) for the different conformational states of cytochrome *c*, the authors were able to fit their high-frequency spectra (marker band regions) with bands attributable to such conformations allowing only small variations to the spectral parameters. Furthermore, they introduced another fitting constraint where the relative intensities of bands attributable to a single species were kept constant throughout the fitting procedure. Lastly, by taking the relative intensity of single marker bands for the different conformers and accounting for differences in Raman cross-sections, Hildebrandt and coworkers were able to get quantitative information on the relative populations of each of the conformers. The authors found a large increase in stability of State II upon binding to negatively charged phospholipid vesicles, arguing that this is the more biologically relevant state on the IMM. In a follow-up study, the same authors show that even a very small

concentration (~5 mol%) of negatively charged phospholipid in a bilayer dominated by neutral phospholipids is enough to induce a noticeable shift to state II. In the same study, the authors investigate the effect of a phase change of the lipids (from a bilayer to an inverted hexagonal structure). To their surprise, such a change in the lipid environment resulted in a relaxation of the structural changes seen for protein bound to phospholipid vesicles.[92]

A study published much later by Hildebrandt and his group in 2004 involves a multi-faceted approach at studying cytochrome c's binding to dioleylphosphatidylglycerol. Here, RR is used complimentary to a variety of other classical methods to characterize the structural states of cytochrome c. Here, they are able to assign different distal ligands to the three different substates of the B2 state – His for the 6cls state, water for the 6chs state, and no ligand in the 5chs state. The identity of the His ligand, be it either of the His33 or the His26 residues, is not clear. The study also performs the measurement at a wide variety of L/P ratios, finding that the B1 state is only dominant up to an L/P of ~10, and it is mostly gone at an L/P higher than 22. The three other substates of B2 show mixed contributions at higher L/P ratios, with the 6cls state being most dominant and the high spin states growing in population only at much higher L/P ratios.[93]

These studies highlight the important fact that negatively charged surfaces create a mixture of different states of cytochrome c, with each one having a characteristic heme configuration. They also exhibited the importance of the L/P ratio when studying such systems. These works grew in number as the number of binding studies of cytochrome c to IMM mimics has increased, but these systems were still of limited biological relevance. As has been mentioned above, there is a preferential interaction between cytochrome c and

the unique IMM phospholipid cardiolipin. Thus, for complete characterization of the biologically relevant states, studies have to be conducted with CL containing IMM mimics – this will be discussed in the next section. This thesis will focus on applying resonance Raman to study the binding of cytochrome *c* to CL containing liposomes.

1.5 – Binding of Cytochrome *c* to Liposomes

While studies of binding to negatively charged electrodes do provide some insight into the potential binding of cytochrome *c* to the IMM, it is far away from simulating a proper mitochondrial membrane surface. Many researchers have instead used CL containing liposomes to mimic the IMM, often using the 20% CL/80% neutral (zwitterionic) background lipid to replicate the same ratios that are observed in the mitochondria. From these studies, it is clear that that cytochrome *c* exhibits several structural changes upon binding to CL-containing liposomes. It has also become clear that the mode of binding is not simple, with both electrostatic and hydrophobic interactions being implicated. Among the hydrophobic interactions, the protein has both been suggested to undergo membrane insertion as well as the facilitating the insertion of one or even two of the CL's acyl chains into the heme cavity. In the following section, the proposed models and the contradictions between them will be briefly outlined.

1.5.1 – Early binding modes and models

The most widely accepted binding models for cytochrome *c* to negatively charged membranes were first proposed by Kinnunen and coworkers in the 1990's.[94-96] They described the binding as a mixture between purely electrostatic interactions and hydrogen

bonding. This proposition was based on experiments via fluorescence resonance energy transfer from specifically labeled CL/phosphatidylcholine (PC) and PG/PC phospholipids to the protein, i.e. a direct measure of the extent of binding. They found two binding sites on the surface of the protein, termed A- and C-sites. The A-site is composed of two lysine residues (K72 and 73) that interact electrostatically with CL's phosphate headgroup. It is thus sensitive to the addition of NaCl due to the screening that Cl^- anions provide on the surface of the protein. The C-site is insensitive to the addition of salt, and was thus attributed to irreversible hydrogen bonding between a protonated CL phosphate headgroup and one of the protein's asparagine residues (N52), an interaction that would require CL to be monoionized (thus achievable at low pH). It should be noted that the authors also allowed for the protonation of the protein instead of the phosphate for C-site binding to occur. Oellerich et al. later proposed two separate hydrophobic patches on the protein that could act as the C-site, shown in Figure 1.5.1.[93] Nantes and coworkers extended this view of binding by exploring the binding at slightly acidic pH, finding another electrostatic binding site composed of multiple lysine residues (K22, K27, and K87) and a histidine residue (H33) that they called the L-site (also reflected in Figure 1.5.1). The authors inferred the existence of this site by observing increases in sample turbidity and vesicle size at lower pH values, with a pK_a of approximately 7.0 as inferred from pH-dependent turbidity kinetics.[97] They attributed the increase in turbidity and vesicle size to liposome fusion in the presence of cytochrome *c* and CL-containing liposomes, which they explained by proposing a new binding site that could act simultaneously with site C to bind two liposomes via one cytochome *c* molecule. For both sites the presence of salt inhibited the binding, contrary to what is observed for site A, indicating that binding at site L is

electrostatic in nature. Due to the pH in the mitochondria being slightly acidic (approximately 6.9, and possibly slightly lower on the negatively charged CL membrane surface), L site binding is most likely physiologically relevant.

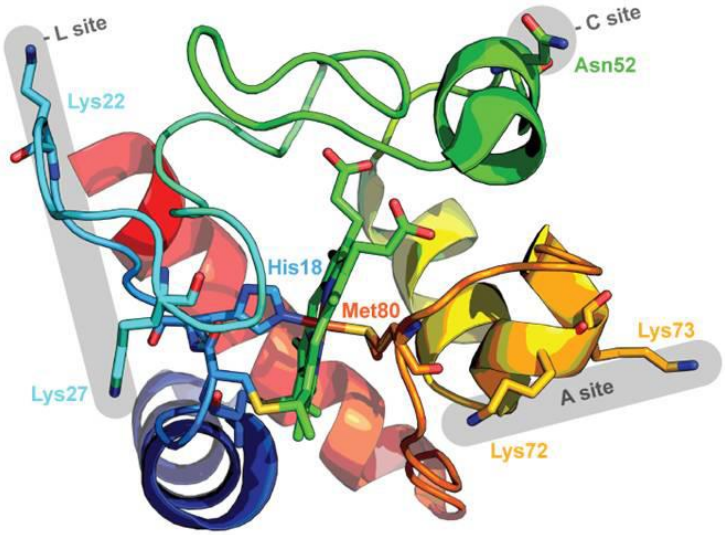

Figure 1.5.1 – Figure depicting the three different binding sites on cytochrome *c*: Kinnunen and coworkers' A and C sites as well as Nantes and coworkers' L-site.[98]

Tuominen et al. expanded on the A- and C-sites by showing that ATP binding influenced C-site bound cytochrome *c* and has no effect on the A-site bound protein. Furthermore, they showed via circular dichroism (CD) measurements that A-site binding has minimal effect on the heme pocket structure. Acidic pH C-site binding, on the other hand, had pronounced effects on the CD spectrum.[99] By measuring CD as a function of CL concentration with 100% CL liposomes to obtain binding isotherms, Sinibaldi et al. discovered two binding steps that had different binding affinities.[100] These were eventually identified as the A-site (high affinity) and the C-site (low affinity). However, they also

found that salt inhibited or reversed the binding at both sites and that ATP competed for A-site binding. Clearly, this is at odds with previously published literature and was thus attributed to inconsistencies in the protocols by Sinibaldi et al.

1.5.2 – Hydrophobic Interactions

In later experiments, Kinnunen and coworkers showed the possibility of extended lipid anchorage, where one of the CL acyl chains inserts itself into the hydrophobic pocket of the protein. Sinibaldi and coworkers showed that two lysines residues (K72 and K79) are involved in the binding by guiding the CL acyl chain into the heme pocket.[101] The proximity of the acyl chain to the heme pocket is what would allow cytochrome *c* to oxidize CL, a process known to occur in the steps before the release of cytochrome *c* into the cytosol. Kalanxhi and Wallace argued this point, proposing a channel close to multiple lysine residues (K72, K73, and K86) that is stabilized by A-site's electrostatic interactions.[102]

Another proposed process is the insertion of the protein into the membrane, something that has been proposed to occur when there is a high degree of protein crowding on the surface of the liposomes. At similar conditions with PG/PC membranes, the spectroscopic results (via previously described Raman studies)[93] were consistent with the protein inserting itself into the membrane, where it allows for hydrophobic interactions. These hydrophobic interactions have been proposed to occur via a hydrophobic patch of residues 81-85, which, due to its close proximity to the M80 ligand, is expected to destabilize the M80 ligation. ESR measurements performed by Kostrzewa et al. showed that multiple lysine residues

(K25, K72, K86, and K87) are also involved in the cytochrome – membrane interaction by performing spin-labeled EPR measurements on DOPG bound cytochrome *c*.[103]

1.5.3 – Recent Binding Models

Recent work by Spiro and co-workers implicated the breaking of a hydrogen bond between residues 26 and 44 (histidine and proline, respectively) as a conformational trigger that leads to multiple changes in the protein's structure that culminate in the dissociation of the M80 ligation to the iron. The authors proposed that this hydrogen bond breaks when H26 interacts with CL, and that it is the subsequent disruption of M80 ligation that allows the protein to act as a peroxidase.[104]

Pletneva and coworkers proposed a more elaborate model to describe the entire unfolding process that cytochrome *c* undergoes upon binding to CL.[105] First, cytochrome *c* is expected to interact electrostatically with the CL headgroups via the many positive residues on its surface, with the most likely candidate being a lysine patch consisting of K73, K73, K86, and K87. Such an interaction and subsequent binding to the surface is what causes the H26 – P44 hydrogen bond to break, which leads to a structural rearrangement that results in the breaking of the M80 ligation, as Spiro and coworkers proposed. These researchers then proposed that the small 60's helix (shown in Figure 1.3.4) interacts with the membrane, laying flat down on the surface of the membrane and pulling 40's loop (also Figure 1.3.4, not labeled) closer to the heme. Furthermore, the C-terminal partially unfolds after inserting itself into the membrane, which in turn causes the N-terminal helix to dissociate away from the C-terminal helix. All of these changes lead to the extended (E)

conformer that Hong et al. described in their earlier works. In those experiments, the authors performed time resolved Förster resonance energy transfer (TR-FRET) on dye-labeled cytochrome *c* that allowed the mapping of dye-to-heme distances and showed evidence for an equilibrium (with submillisecond exchange rates) between two different conformers.[106] One of those states is a compact molten globule like state they termed the C-state, and another a much more extended conformer they termed the E-state. This is depicted in Figure 1.5.2.

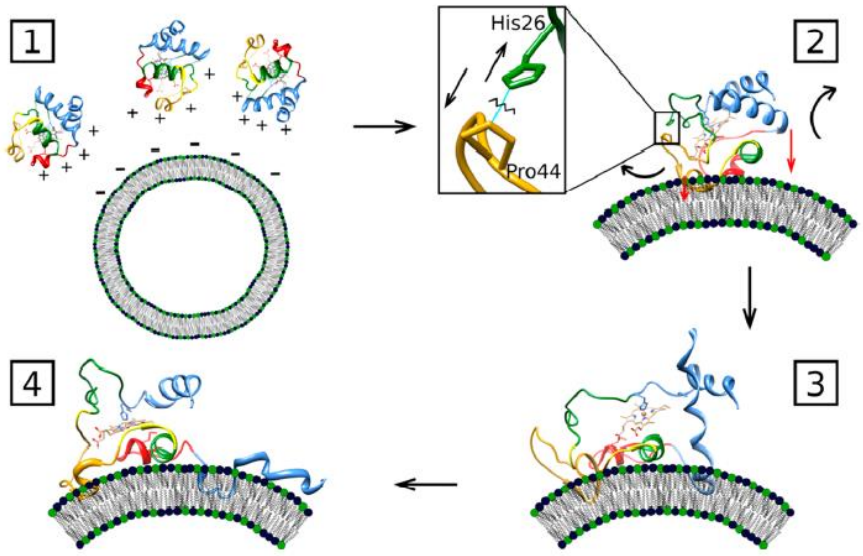

Figure 1.5.2 – Proposed conversion into a compact state (2) and subsequent conversion to the extended state (3-4) by Pletneva and coworkers.[105]

More recently, Pandiscia and Schweitzer-Stenner proposed a binding model that came as a result of a global fitting procedure to circular dichroism, UV/Visible absorption, fluorescence spectroscopy and fluorescence anisotropy response data produced by the binding of cytochrome *c* in the presence and absence of NaCl to liposomes of different CL lipid content (20, 50, and 100 mol% TOCL, with the remaining fraction DOPC). With the

model, they proposed a CL-dependent unimolecular equilibrium for cytochrome *c*. First, cytochrome *c* binds to the membrane and retains a native-like conformation that does not fluoresce (hence the terminology of non-fluorescing, or nf-, state). This state dominates at low lipid-to-protein ratios, and is reminiscent of Pletneva's C-state. The nf-state, as proposed, is not a single state but rather an ensemble of compact conformations, with some subsets of this population retaining the native M80 ligation and others losing it. However, as the CL concentration is increased, there is shift to a partially unfolded fluorescing state (termed the f-state) as the protein undergoes a conformational transition through which the fluorescing W59 moves away from heme. This state encompasses both hexa- and pentacoordinated states of the heme group, with the former being dominant and the latter being observed during cytochrome *c* binding to 100% TOCL liposomes.[107] This model provided an explanation as to how cytochrome *c* was able to balance both of its functions, as the concentration of CL that cytochrome *c* comes into contact with are vastly different between normal operating conditions and an apoptotic cell. The binding scheme is illustrated in Figure 1.5.3.

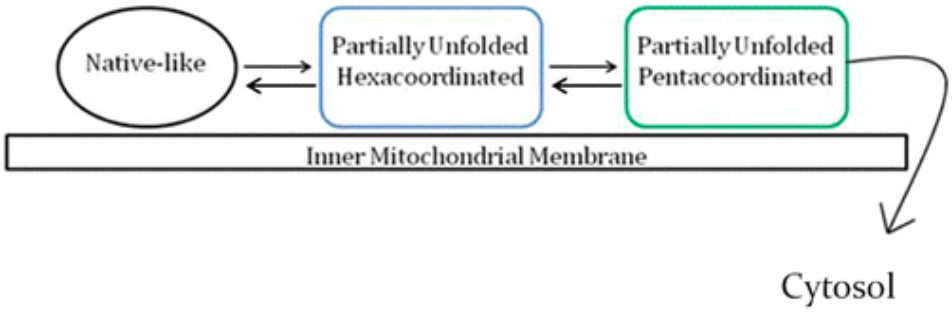

Figure 1.5.3 – Binding scheme proposed by Pandiscia and Schweitzer-Stenner, describing the process as a CL dependent equilibrium between a native-like (nf-) state and non-native (f-) states.[107]

1.6 – Research Outlook

There have been many studies published on the cytochrome *c* – cardiolipin system in an attempt to characterize the protein's involvement in apoptosis. From these studies it is clear that cytochrome *c* can undergo rather extensive conformational transitions, some of which can make the protein more likely to act as a peroxidase. However, with multiple binding models and sites proposed with a consensus on the highly electrostatic nature of this binding, there is still no clear consensus as to what the oxidation state of CL is. The model of Kates et al. that proposed the bicyclic stabilization of the monoionized state has been widely accepted and supported by calculations, contrary to what many early and some recent studies have indicated. Also, there have been a rather limited number of studies looking at the resonance Raman response during binding, which is initially surprising simply due to its usefulness in elucidating the many possible conformational states of heme proteins as has been outlined in the works of Spiro and Hildebrandt.

The primary focus of this thesis will be a vibrational spectroscopy approach of resolving some of these issues, where an infrared spectroscopic analysis of the ionization state of CL and Raman analysis of cytochrome *c* binding to CL-containing liposomes will both be presented. With infrared spectroscopy, the phosphate group vibrations were specifically analyzed as a function of pH for different liposomes contents (100% CL, 20%/80% CL to PC, and 100% PC). Phosphate groups in phospholipids are highly sensitive to the ionization state, as the symmetric/asymmetric $(PO_2)^-$ vibrations observed in the ionized form are lost upon protonation to O=P-OH, and this is easily tracked with infrared absorption. In support of the experimental data, DFT normal mode analysis will be presented as well. As for the

study of binding itself, the resonance Raman response of cytochrome *c* was measured as a function of CL-liposome concentration. The photoreduction phenomenon, a reduction of the protein upon interaction with the laser excitation, was turned into a powerful tool to study the binding. Through spectral decomposition methods in the mold of those presented by Hilderbrandt and coworkers,[92] a quantitative assessment of the binding will be presented and compared to the model of Pandiscia and Schweitzer-Stenner.[107]

CHAPTER 2 – THEORY BEHIND SPECTROSCOPIC METHODS

2.1 – Theory of Infrared Spectroscopy

Infrared spectroscopy uses the absorption of infrared light to probe the vibrational modes of a molecule. The theory of infrared spectroscopy is discussed here briefly, with the derivation of the selection rules in the context of the harmonic oscillator. The harmonic oscillator wavefunctions are obtained by solving the Schrödinger equation with the potential energy operator $V = kx^2/2$, i.e. the harmonic potential energy of a spring system. The stepwise solution has been shown elsewhere, with the following set of wavefunctions satisfying the differential equation:

$$\psi_n = \left(\frac{\alpha}{\pi}\right)^{\frac{1}{4}} \left(\frac{1}{\sqrt{2^n n!}}\right) e^{-\frac{\alpha x^2}{2}} H_n \qquad where\ \alpha = \frac{m\omega}{\hbar}\ and\ \omega = \sqrt{\frac{k}{M}}$$

where n is the quantum number, M is the reduced mass of the spring system, ω is the frequency of the vibration, k is the spring constant, x is the spatial coordinate displacement (in reference to the equilibrium position), and H_n are the physicists' Hermite polynomials.

The harmonic oscillator has been often used to approximate molecular vibrations, and it can also be used to explain the selection rules for infrared spectroscopy.

The transition probability from state n to m depends on the transition dipole moment integral, μ_{nm}:

$$\mu_{nm} = \int \psi_m^* \mu \psi_n dq$$

where μ is the dipole moment of the molecule and q refers to the normal mode coordinates. This dipole moment can be expanded in first order Taylor series:

$$\mu \approx \mu_0 + \left(\frac{\partial \mu}{\partial q}\right)_{q_0} q$$

Inserting this approximation into the transition dipole moment integral gives rise to the following:

$$\mu_{nm} = \mu_0 \int \psi_m^* \psi_n dq + \left(\frac{\partial \mu}{\partial q}\right)_{q_0} \int \psi_m^* q \psi_n dq$$

Orthonormality dictates that the first term is zero when m≠n, meaning that the transition dipole moment for infrared transitions only depends on the second term. With the harmonic oscillator wavefunctions:

$$\mu_{nm} = A_m A_n \left(\frac{\partial \mu}{\partial q}\right)_{q_0} \int H_m H_n q e^{-\alpha q^2} dq$$

Where A_m and A_n are the constants that are associated with each wavefunction. For the transition to occur, this term must be non-zero. This means that the spatial derivative of the dipole moment must be non-zero, i.e. there must be a change in the dipole moment.

Furthermore, the integral itself must be non-zero, which only occurs under the condition that $m = n \pm 1$ due to the first order q term in the integrand, which constricts the product of the Hermite polynomials to odd functions only. These two conditions are the classical selection rules for infrared transitions. Expansions of the dipole moment to higher orders as well as anharmonicity lead to the relaxation of the latter selection rule, normally observed as overtones in the infrared spectra.

It should be noted that a group theory approach can be taken to find which vibrational modes are infrared active. The irreducible representation of the vibrational mode, i.e. the excited vibrational state of the molecule, must transform as one of the spatial coordinates (x, y, or z) in the point group basis of the ground state, as can be inferred from the first order q term in the transition dipole moment integrand (since the ground state is totally symmetric, the only way to achieve a totally symmetric transition dipole moment integral with the q term is if the excited state transforms as one of x, y, or z). Carbon dioxide, a molecule of a $D_{\infty h}$ point group, has four total vibrational modes, transforming as A_{1g}, A_{1u}, and E_{1u} (or Σ^{+}_{g}, Σ^{+}_{u}, and Π_{u}, respectively). Out of these, A_{1u} transforms as z while E_{1u} modes transform as x and y, meaning that they are infrared active while the A_{1g} mode is not. These correlate with the asymmetric stretch of the carbon dioxide molecule (A_{1u}) and the degenerate bending modes (E_{1u}) being IR active while the symmetric stretch (A_{1g}) is not (it is Raman active, however). Of course, this is easy to deduce without a group theory argument by the basic concept of a need in a change of the dipole moment, but such a simplified analysis can get rather complicated as the molecules grow larger. It should be noted that any vibrational modes of molecules with an inversion center that have a *gerade* irreducible representation are generally IR inactive.

Infrared spectroscopy has been classically used in identifying the presence of functional groups in the molecule, e.g. a sharp band around 1700 cm^{-1} being indicative of the presence of a carbonyl group. However, it should be noted that for most molecules, observed vibrational modes should not always be attributed to the isolated vibrations of just the functional group, as many vibrations are coupled to others.

2.2 – Four Orbital Model

In order to properly describe resonance Raman spectroscopy, Gouterman's four orbital model for porphyrins must first be briefly discussed. This model aims at describing the UV/Visible spectrum of porphyrins, consisting of an intense B band and a much weaker Q band as shown in Figure 2.2.1.

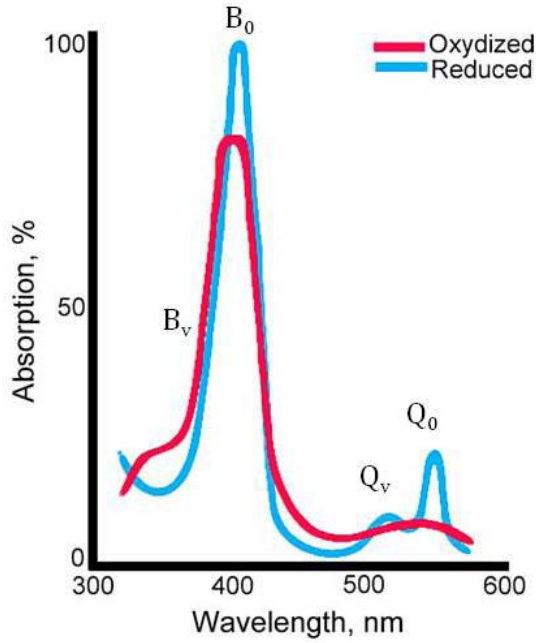

Figure 2.2.1 – Optical absorption spectrum of both oxidation states of cytochrome *c*. Notice the clear difference in intensities between the B and Q bands.

Following the calculations of Longuett-Higgins et al., the two highest occupied molecular orbitals (MO's) for a porphyrin in D_{4h} symmetry are of A_{1u} and A_{2u} symmetries, whereas the lowest unoccupied MO is of a doubly degenerate E_g symmetry. This leads to four possible electronic configurations of the excited state. However, if the A_{1u} and A_{2u} states are assumed to be accidentally degenerate, the resulting 50:50 mixing results in two degenerate electronic configurations, $Q^0_{x,y}$ and $B^0_{x,y}$, both in E_u symmetry, described as follows:

$$\begin{vmatrix} Q_x^0 \\ Q_y^0 \\ B_x^0 \\ B_y^0 \end{vmatrix} = \frac{1}{\sqrt{2}} \begin{vmatrix} |A_{2u}E_{gx}\rangle + |A_{1u}E_{gy}\rangle \\ |A_{2u}E_{gy}\rangle - |A_{1u}E_{gx}\rangle \\ |A_{2u}E_{gx}\rangle - |A_{1u}E_{gy}\rangle \\ |A_{2u}E_{gy}\rangle + |A_{1u}E_{gx}\rangle \end{vmatrix}$$

Where A_aE_{gb} denotes a one electron transition from A_a to the b component of the E_g MO. Since these states are degenerate, the configurational interactions splits them by an amount δ, leading to the observed positions of the Q_0 and B_0 bands. It can then be shown via the electronic dipole transition moments for the two excited configurations that the Q state is practically forbidden. However, the Q band is clearly observable in the spectra of many porphyrins. This is most likely due to the $A_{1u}E_{gb}$ and $A_{2u}E_{gb}$ not being entirely degenerate, leading to the unmixing of 50:50 mixed states. This can be accounted for by introducing an off-diagonal interaction parameter δ_{A1g} in the perturbation Hamiltonian and applying first-order perturbation theory. The resulting electronic configurations are:

$$\begin{vmatrix} Q_x \\ Q_y \\ B_x \\ B_y \end{vmatrix} = \begin{vmatrix} \cos\nu\,|Q_x^0\rangle - \sin\nu\,|B_x^0\rangle \\ \cos\nu\,|Q_y^0\rangle - \sin\nu\,|B_y^0\rangle \\ \sin\nu\,|Q_x^0\rangle + \cos\nu\,|B_x^0\rangle \\ \sin\nu\,|Q_y^0\rangle + \cos\nu\,|B_y^0\rangle \end{vmatrix}$$

where ν is an unmixing parameter defined by:

$$\tan\nu = \frac{\delta_{A_{1g}}}{E_B^0 - E_Q^0}$$

where E^0_a refers to the energy of the non-perturbed (50:50 mixed) *a* electronic configuration. With this approach, it can also be showed that the splitting between the Q and B states is enhanced due to the unmixing, and that there is a consequent redistribution of intensities from the B to the Q band.

So far, only the electronic contributions have been discussed. There are, however, vibronic contributions to the spectra, as well, leading to a defined Q_v band and the asymmetry of the B band on the high energy side. Without details on the subject, both intrastate (Franck-Condon and Jahn-Teller) and interstate (Herzberg-Teller) vibronic coupling mechanisms contribute to the vibronic structure of the electronic spectra. It should be noted that interstate coupling causes an increase in intensity of the Q_v region, accounting for approximately 80% of its intensity.

2.3 – Theory of Resonance Raman Spectroscopy

The theory of Raman scattering has been well-established since the discovery of the Raman effect in 1929, and it is described in detail elsewhere.[108-110] In short, Raman scattering

occurs as a spontaneous process that depends on the induced dipole moment $\vec{\mu}$, which in turn depends on the electric field component $\vec{E}$ of the incoming radiation and the molecule's polarizability tensor $\hat{\alpha}$ as follows, described here in first order:

$$\vec{\mu} = \hat{\alpha}\vec{E}$$

where the electric field component of the incoming radiation can be described as follows:

$$\vec{E} = E_o \cos(2\pi v_0 t)$$

where t is time and ν_0 is the frequency of the incoming radiation. At the same time, the vibrational coordinates of the molecule during a vibration can be expressed as follows, per the harmonic oscillator:

$$Q = Q_{max} \cos(2\pi v_{vib} t)$$

where Q_{max} is the amplitude of the vibrational displacement and ν_{vib} is the frequency of the vibration. To account for changes in the polarizability during molecular vibrations, the polarizability can be expanded in a Taylor series to first order around the vibrational coordinates:

$$\hat{\alpha} = \widehat{\alpha_0} + \frac{\partial \hat{\alpha}}{\partial Q} Q$$

Substituting these expressions into the induced dipole moment equation gives rise to the following equation:

$$\vec{\mu} = \hat{\alpha}_0 E_o \cos(2\pi \upsilon_0 t) + \frac{\partial \hat{\alpha}}{\partial Q} Q_{max} E_o \cos(2\pi \upsilon_0 t) \cos(2\pi \upsilon_{vib} t)$$

$$= \hat{\alpha}_0 E_o \cos(2\pi \upsilon_0 t) + \frac{\partial \hat{\alpha}}{\partial Q} \{\cos[2\pi(\upsilon_0 - \upsilon_{vib})t] + \cos[2\pi(\upsilon_0 - \upsilon_{vib})t]\}$$

The first term in this equation describes elastic Rayleigh scattering, whereas the second term describes both Stokes and anti-Stokes scattering mechanisms characteristic of Raman scattering. Here, it is clear that Raman scattering requires a change in the polarizability tensor as a function of the vibration, i.e. the vibrational excited state representation must transform as any one of the second-order spatial coordinates in the point group of the ground state for a molecule.

The main measurable Raman scattering result is scattered photons with energy losses corresponding to the molecule's vibrational modes. Normal Raman scattering occurs on the order of 1 per 10^5 photons, with the rest being Rayleigh scattered, thus requiring powerful laser lines to achieve measurable Raman scattering. However, resonance Raman scattering leads to an enhancement of this effect. It occurs when the incoming radiation's energy matches the energy of an electronic transition, leading to all vibrational modes that are vibronically coupled to the electronic transition to be resonance enhanced.

The polarizability tensor elements for resonance Raman is calculated using the Kramers-Heisenberg-Dirac equation, as follows:

$$\hat{\alpha}_{\rho,\sigma} = \sum_i \frac{\langle f|\mu_\rho|i\rangle\langle i|\mu_\sigma|g\rangle}{E_i - E_g - \hbar\omega - i\Gamma_i} + \frac{\langle f|\mu_\sigma|i\rangle\langle i|\mu_\rho|g\rangle}{E_i + E_g - \hbar\omega - i\Gamma_i}$$

where ρ, σ=x,y,z are label the axis of a three-dimensional coordinate system defined by the directions of the transition dipole moments μ_ρ, μ_σ; *g*, *f*, and *i* refer to the total wavefunctions

of the ground, final, and intermediate states, respectively; E_i and E_g refer to the energies of the intermediate and ground states, respectively; $\hbar\omega$ refers to the energy of the incoming radiation, and Γ_i is the damping constant associated with the intermediate state. The first term describes the resonance contribution, while the second term describes the non-resonance effects. The numerator in both terms describes two sequential electronic transitions (from *g* to *i*, then *i* to *f*). Clearly, when the excitation energy lies close to the energy difference between the ground and intermediate states, the resonance term dominates and the non-resonance term can be neglected.

In order to specifically describe resonance Raman scattering in porphyrins, the total vibronic wavefunction must be considered. Through the Born-Oppenheimer approximation the vibrational wavefunction can be separate from the electronic one, with the vibronic wavefunction expressed as follows:

$$\psi_{e,v} = \theta_e(r, Q)\varphi_{e,v}(Q)$$

where ψ refers to the vibronic wavefunction, θ labels the electronic wavefunction for a set of nuclear coordinates *Q* and electronic coordinates *r*, and ϕ refers to the vibrational wavefunction of the electronic state *e*. Due to the Born-Oppenheimer approximation, the Q coordinate is fixed in the electronic wavefunction. Through an expansion of the electronic wavefunction with respect to the nuclear coordinates in first order (termed Herzberg-Teller expansion), the classical Albrecht theory can be derived to describe vibronic coupling. This leads to the classical A and B terms, with the A term describing the intrastate Franck-Condon coupling mechanism whereas the B term accounts for the intrastate coupling, with the final polarizability tensor element being the summation of the

two terms. Such an approach, however, is adiabatic in that it assumes a purely electronic energy of the electronic manifold in the denominator of the KHD equation. It also does not account for multimode mixing of all non-totally symmetric Raman modes. In order to account for these, a third-order perturbation theory approach must be applied to the vibronic wavefunctions. This was first applied to porphyrins by Shelnutt and Shea,[111] followed by Unger et al.[83] as well as Schweitzer-Stenner et al.[112] With this, the following expression for the polarizability tensor elements can be obtained (with multi-mode mixing terms neglected):

$$\hat{\alpha}_{\rho,\sigma} = \sum_{m,l} \frac{\langle g|\mu_\rho|l\rangle \left\langle l\left|\frac{\partial H_{el}}{\partial Q_r}\right|m\right\rangle \langle m|\mu_\sigma|g\rangle\langle 1|Q_r|0\rangle}{\left(E_{0,0}^{l,r,\lambda} - \hbar\omega - i\Gamma_{0,0}^{l,r,\lambda}\right)\left(E_{0,0}^{l,r,\lambda} - E_{0,1}^{m,r,\lambda}\right)}$$

$$+ \sum_{m,l} \frac{\langle g|\mu_\sigma|l\rangle \left\langle l\left|\frac{\partial H_{el}}{\partial Q_r}\right|m\right\rangle \langle m|\mu_\rho|g\rangle\langle 1|Q_r|0\rangle}{\left(E_{1,0}^{l,r,\lambda} - \hbar\omega - i\Gamma_{1,0}^{l,r,\lambda}\right)\left(E_{1,0}^{l,r,\lambda} - E_{0,1}^{m,r,\lambda}\right)}$$

Here, r refers to the Raman active vibrational mode; m and l refer to separate equilibrium electronic manifolds while g refers to the ground state electronic manifold; $\frac{\partial H_{el}}{\partial Q_r}$ is the vibronic coupling operator, and numbers 0 and 1 refer to the vibrational quantum numbers. The formalism assumes that the scattering process starts in the vibrational ground state of the electronic ground state. The second and fourth terms in the numerator of both sums are elements of the vibronic coupling matrix, and they ultimately govern the resonance Raman activity.

2.3.1 – Selection Rules for Raman

For the Raman effect to be observed, the polarizability tensor must change as a consequence of the vibration, as has been deduced above. This is best determined by a group theory approach, where the irreducible representation of the vibrational mode must transform as a second order spatial coordinate for the mode to be Raman active.

As was stated before, the vibronic coupling matrix elements govern the Raman activity as presented above. Since the excited state for porphyrins (in D_{4h} symmetry) have E_u symmetry per the four orbital model, the vibronic coupling parameter must transform as one of the subsets of the product $E_u \otimes E_u$ (A_{1g}, A_{2g}, B_{1g}, or B_{2g}). In D_{4h} symmetry, this leads to 35 Raman active vibrational modes (9 A_{1g}, 8 A_{2g}, 9 B_{1g}, and 9 B_{2g}) for the heme group in cytochrome *c*, all of which are in-plane vibrations. However, depending on the excitation, modes of different symmetries can be preferentially enhanced. For example, with excitation in the Soret band region, the A_{1g} modes are predominantly enhanced. Of course, there are different coupling mechanisms to consider. A_{1g} modes can also induce Herzberg-Teller (QB/interstate) coupling. This leads to noticeable intensities if the excitation wavelength is between the B_0 and Q_v bands. Both Frank-Condon (FC) and Jahn-Teller (JT) coupling are intrastate coupling mechanisms, with the former contributing to the A_{1g} modes as well. With B_{1g} and B_{2g} modes, both HT and JT coupling contribute. For the A_{2g} modes, only HT coupling contributes.

2.3.3 – Resonance Raman Scattering in Porphyrins

For porphyrins, resonance Raman scattering is a powerful tool. This is owing to the many structurally sensitive vibrations that are found in the high frequency region (1300-1700 cm^{-}

[1]), which are mainly assignable the vibrational modes of the tetrapyrrole macrocycle. A very prominent mode is ν_4 (using notation of Abe et al.), an A_{1g} oxidation state marker band exhibiting a ~13 cm^{-1} shift upon changes in oxidation state. Such a drastic difference has been attributed to an increase in electron density back donation from the iron center to the macrocycle's π^* orbitals upon reduction. In the same region, ν_3 and ν_2 are other A_{1g}-type structure sensitive modes that can also be used as spin-marker bands. In the same region, ν_{10} and ν_{11} are oxidation markers of the B_{1g}-type, with the former also utilized as a spin marker band. Also, the ν_{19} (of B_{2g} symmetry) is found in the same region, often complicating analysis for the spectral region where ν_{11}, ν_2, and ν_{19} overlap while giving little structural information. The frequencies of these marker bands for different heme configurations is tabulated in Table 2.1:

Table 2.1. Structurally sensitive marker bands in the high frequency region of the resonance Raman spectra of cytochrome *c*. These are the canonical band positions, presented with notation per Abe et al.

Heme Configuration		**High Frequency Marker Bands Frequencies (cm^{-1})**					
Oxidation	**Heme**	ν_2	ν_3	ν_4	ν_{10}	ν_{11}	ν_{19}
Fe^{3+}	*6cLS*	1584	1502	1374	1635	1562	1582
	6cHS	1570	1485	1370	-	-	-
	5cHS	1577	1497	1371	1623	-	-
Fe^{2+}	*6cLS*	1591	1491	1361	1621	1548	1585
	5cHS	1572	1470	1354	1606	1547	-

Here, it is evident that ν_3, ν_4, ν_{10}, and ν_{11} can be used as oxidation state markers. However, due to the spectral overlap between ν_2, ν_{11}, and ν_{19}, the use of ν_{11} band as an oxidation state marker band with excitation in the B-band region depends on the spectral resolution and the signal-to-noise ratio. Both ν_2 and ν_3 are great spin and ligation markers, and ν_{10} is a

great spin marker band due to it being somewhat isolated. Of these, however, ν_3 and ν_4 are highly isolated and can thus act as very isolated oxidation and spin markers.

The heme in cytochrome *c* experiences a lot of steric interactions with the protein around it as well as the heme's substituents, introducing some out-of-plane deformations to the porphyrin that lower the symmetry down from D_{4h}. These distortions do have some influence on the high frequency marker bands, but the most prominent change is observed in the low frequency part of the spectrum. Out-of-plane vibrational modes are Raman forbidden in D_{4h} symmetry because they transform as *ungerade* (except for E_g out-of-plane modes, which are Raman active but are not resonance enhanced). However, these modes become resonance Raman active upon introduction of symmetry lowering out-of-plane deformations such as ruffling (the natural state of the heme in cytochrome *c*) or doming (the predominant deformation found in oxygen-carrying proteins such as hemoglobin and myoglobin). These deformations can be quantified by a structural decomposition method proposed by Shelnutt and coworkers,[34, 113] where the crystal structure of the protein is used to characterize and quantify the in-plane and out-of-plane distortions.

CHAPTER 3 – MATERIALS AND METHODS

3.0 – Sample Preparation

3.0.1 – Liposome Preparation

Both 1,1′2,2′-tetraoleyl cardiolipin (TOCL) and 1,2-dioleyl-*sn*-glycero-3-phosphocholine (DOPC) were purchased from Avanti Polar Lipids (Alabaster, AL) as sodium salts. 100% TOCL and 20% TOCL/80% DOPC liposomes were prepared by adopting the protocol of Hanske et al.[75] After being dissolved in a 2:1 methanol/chloroform mixture in a round bottom flask, the solutions were rotary evaporated for half an hour until a dry lipid film formed. The flask was then placed into a sealed calcium chloride dessicant overnight. The film was rehydrated with a 25 mM HEPES buffer to achieve a final lipid concentration of either 10 mM (infrared experiments) or 25 mM (resonance Raman experiments). The resulting solution was ultrasonicated in an ice bath for an hour at 100 W. The sonicated sample was centrifuged at 12,000 rpm for 40 min to remove traces of titanium from the sonifier tip. The supernatant was extracted and left to stabilize overnight. All liposome solutions were stored under nitrogen to prevent oxidation.

3.0.2 – Liposome Follow-Up for Infrared Experiments

The pH of all solutions was adjusted by adding small aliquots of 1.25 M hydrochloric acid (HCl) or 1.25 M sodium hydroxide (NaOH), and then measured with an Accumet® pro pH probe. The target pH range was 5–12 for DOPC and 2–12 for TOCL. The total lipid concentration for all experiments was 10 mM. The CL-solution was checked with light scattering, making sure that a homogeneous distribution with a diameter of ca. 50-60 nm was obtained.

3.0.3 – Cytochrome c Preparation

All cytochrome c stock solutions were prepared in line with the protocol first reported by Alessi et al.[84] First, unpurified cytochrome *c* obtained from Sigma-Aldrich (St. Louis, MO) was dissolved in 25 mM HEPES buffer. After bringing the pH of the solution to 11.5, a minimal amount of potassium ferricyanide was added to the system to completely oxidize the protein. After the protein sample was allowed to oxidize for approximately one hour at 5 °C, the solution was passed through a Sephadex column (pre-treated with potassium ferricyanide to account for the reducing nature of the column) to purify the protein sample of any hexacyanoferrates. The concentration of the final cytochrome sample was determined by measuring the absorbance of the Soret band.

3.0.4 – Preparation of Protein/Liposome Mixtures

Samples at each lipid-to-protein ratio were prepared by adding a constant volume of a protein stock to samples with varying liposome content, with a final protein concentration of 100 μM adjusted by adding HEPES buffer before adjusting the final pH to 7.0 with minor additions of HCl when needed. All samples were prepared fresh and allowed to equilibrate for 30 min prior to any measurements.

3.0.5 – Preparation of Photoreduction-Prone Samples

To achieve photoreduction, potassium ferrocyanide (Aldrich Chemical Company) was added in a 4:1 ratio during the preparation of the protein/liposomes mixtures. This ratio was selected based on multiple measurements, being the lowest ratio where complete photoreduction was occurring.

3.0.6 – Dynamic Light Scattering

Particle radii measurements were obtained using a Horiba Lb 500 Dynamic Light Scattering Particle Size Analyzer (Edison, NJ). A 10 mm path length quartz cuvette was used to collect data at room temperature.

3.1 – Spectroscopic Measurements

3.1.1 – Infrared Spectroscopy

All spectra were obtained with a PerkinElmer Spectrum One FT-IR spectrometer, focused on the spectral region between 1000 and 1300 cm^{-1}, which contains bands assignable to vibrations of the phosphate groups. A transmission cell made of two barium fluoride crystals with 50 μm Teflon spacer was used to hold the sample while 32 background corrected scans were taken over a span of about 2 min. Furthermore, background scans of the buffer itself were taken under the same conditions and subtracted from the liposome spectra.

3.1.2 – Resonance Raman Spectroscopy

All Raman spectra were obtained by using a Renishaw RM-1000 Ramascope with a BH-2 confocal Raman microscope. All spectra were obtained with 442 nm excitation (HeCd, Kimmon) with a final laser power of approximately 20 mW at the sample, and the spectrometer was calibrated by a silicon wafer by setting the silicon peak to 520.0 cm^{-1}. Multiple spectra for each sample were taken (and later averaged in MULTIFIT) after relocating the laser focal point in between subsequent spectra to reduce any effects from prolonged laser exposure.

For all Raman spectra of cytochrome c with liposomes, Mie scattering affects the spectral background and complicates spectral analysis. To correct this, spectra of pure liposomes at the same concentration as in the protein sample were taken and subtracted from protein/liposome spectra. This corrected the baseline and made the spectral analysis straightforward.

CHAPTER 4 – RESULTS AND DISCUSSION

This section is reproduced in part from the following publications:

Dmitry Malyshka, Leah A. Pandiscia, and Reinhard Schweitzer-Stenner. Cardiolipin containing liposomes are fully ionized at physiological pH. An FT-IR study of phosphate group ionization. *Vibrational Spectroscopy.* **2014,** *75*, 86.

Dmitry Malyshka and Reinhard Schweitzer-Stenner. Ferrocyanide-Mediated Photoreduction of Ferricytochrome c Utilized to Selectively Probe Non-native Conformations Induced by Binding to Cardiolipin-Containing Liposomes. *Chemistry - A European Journal.* **2017**, *23*, 1151.

Bridet Milorey, Dmitry Malyshka, and Reinhard Schweitzer-Stenner. pH Dependence of Ferricytochrome *c* Conformational Transitions during Binding to Cardiolipin Membranes: Evidence for Histidine as the Distal Ligand at Neutral pH**.** *Journal of Physical Chemistry Letters*, **2017**, *8* (9), 1993.

4.1 – Introduction

Cytochrome *c* is now known to be a multifaceted protein localized in the mitochondria. In a healthy cell, it is responsible of shuttling an electron from Complex III (cytochrome bc_1 complex, i.e. cytochrome *c* reductase) to Complex IV (cytochrome *c* oxidase), a role it can perform only in its native conformation due to the rather high redox potential that the methionine ligand enforces. This shuttling process drives the pumping of protons into the intermembrane space from the matrix, creating an electrochemical gradient that drives the formation of ATP at the ATP synthase complex. However, relatively recent studies have revealed its vital role in apoptosis. Upon interacting with cardiolipin, cytochrome *c* adopts a peroxidase-active conformation, oxidizes cardiolipin, and escapes the mitochondria through a series of biochemical steps where it can bind to $Apaf_1$. The question as to what concentration of cardiolipin causes such an effect as well as the specific details of these conformational transitions are still outstanding, and this has led many groups to study the binding of cytochrome *c* to CL membranes, namely liposomes and vesicles of varying sizes. As outlined in detail above, much of the information regarding the different binding sites and binding modes has been found from these binding studies, but some questions still stand.

The goal of this study is to answer some of the outstanding questions. The protonation state of CL under physiological conditions has been a contested topic, with some subscribing to the bicyclic model of the monoionized structure[59] over the expected doubly ionized form of cardiolipin as the classical studies have suggested.[61] It is vital to resolve this issue in reference to the cytochrome *c* – CL interactions due to the highly electrostatic nature of these effects as well as the requirement for CL (or protein) protonation for the C site binding to occur. To resolve this, the phosphate group vibrations of both CL and PC

vesicles are probed via infrared spectroscopy over the pH range. The data indicate that CL undergoes a protonation below the pH of 5.0 (approximately the same pH where Kinnunen and co-workers observed C-site binding),[94] but no deprotonation was observed between the pH values of 7 and 12. This is clearly at odds with the bicyclic model, and indicates that CL in CL-containing membranes is doubly ionized at neutral pH. Along with the infrared studies, DFT normal mode calculations are used to support the experimental data.

Furthermore, it is clear that cytochrome *c* undergoes conformational transitions upon binding to CL membranes, but it is not clear as to which of these observed changes cause the protein to gain peroxidase activity. The recently published binding model by Pandiscia and Schweitzer-Stenner,[107] supporting the model of Pletneva and co-workers,[105] described the conformational transitions as a CL-dependent equilibrium between a native-like non-fluorescing (nf-) state and partially unfolded pentacoordinated and hexacoordinated fluorescing (f-) states. The conformational identity of these states, however, was not entirely clear, with no direct evidence yet presented as to what ligand (histidine or lysine) replaces the native methionine. To resolve this, resonance Raman spectroscopy was utilized to study the conformational transitions of cytochrome *c* on the CL-membrane surface. A new method was developed where photoreduction, a classically detrimental phenomenon in the studying of heme proteins, was used to elucidate the bound non-native conformers of the protein. The spectral data indicates that most of the protein adopts a low-spin configuration if the binding occurs at neutral pH. When exploring the binding at the pH of 6.5 (where L-site binding is expected to compete with the A-site and histidine is protonated), there are clear differences that can be observed. The protein exists predominantly in a high-spin state (both pentacoordinated and water-ligated

hexacoordinated). Furthermore, this new type of binding is shown to be electrostatic in nature, consistent with the L-site binding of Nantes and coworkers.[97] Due to this difference existing when histidine is protonated, these data point to histidine being the likely ligand replacing the native methionine during CL-induced unfolding at neutral pH.

4.2 – Infrared Results in the Study of CL's Phosphate Group Ionization

To elucidate the degree of phosphate head group protonation of CL and PC, the primary focus was on the part of the spectrum between 1000 and 1300 cm-^{1}. Generally, a rather broad band in the region between 1200 and 1300 cm^{-1} is assigned to asymmetric OPO stretch combinations, whereas the broad and asymmetric band between 1000 and 1100 cm^{-1} is attributed to the symmetric OPO stretch of the deprotonated phosphate group.[114] Figure 4.2.1 exhibits these spectral regions for 100% TOCL and 100% DOPC, respectively, recorded at pH 5.0. TOCL has a phosphate content twice that of DOPC, and it is reflected in its spectrum being roughly twice as intense. DOPC and TOCL spectra measured at different pH were self-consistently fitted with a spectral model comprising of a minimal amount of Gaussian bands for which the wavenumber positions and halfwidths were kept constant, with the resulting fit shown in Figure 4.2.1. The thus performed spectral decomposition should be regarded as a minimal model, which cannot fully account for the spectral density in the investigated frequency region. As is shown below, however, the decomposition allowed the narrowing of the spectral region which is dominated by contributions assignable to P-O and P=O stretching modes.

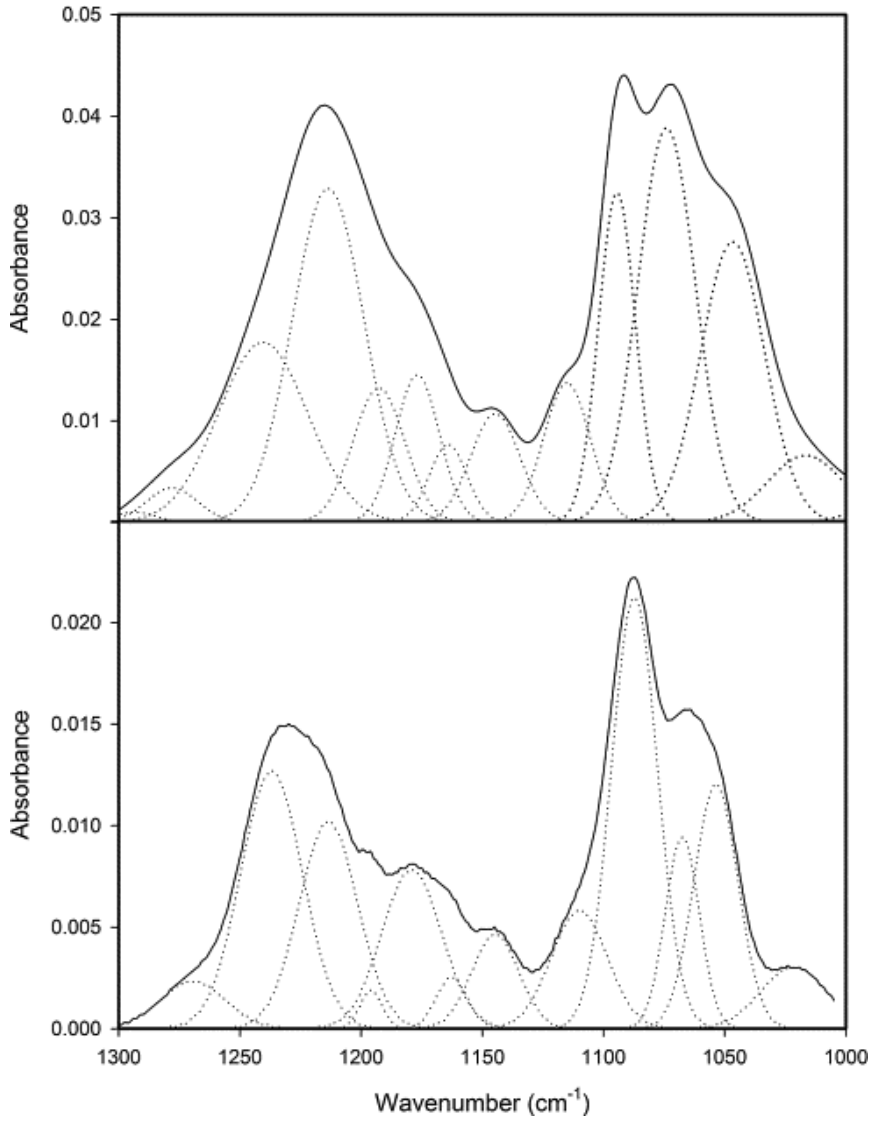

Figure 4.2.1 - Decomposed spectra of 100% cardiolipin liposomes (top) and 100% phosphatidylcholine liposomes (bottom) at a pH of 7. The decomposition bands shown here are the ones used for the fitting model for the respective liposome spectra across the pH range, obtained as described in the text.[115]

Figs. 4.2.2 and 4.2.3 display the integrated intensities of the obtained bands of DOPC and TOCL as a function of pH. Within the limit of experimental accuracy, the DOPC band

intensities do not show any significant pH-dependence. This was, of course, expected due to the extreme pK_a values required to obtain any pH related changes such as deprotonation of the choline or protonation of the phosphate. The small variations of the data points can be considered as a measure of their statistical uncertainty. For TOCL, however, the situation is different. Bands at 1094 cm^{-1}, 1073 cm^{-1} and 1213 cm^{-1}, the intensity of which decrease as function of pH below pH 5, while two bands at 1016 cm^{-1} and 1192 cm^{-1} become concomitantly more intense. There is no significant pH-dependence of the TOCL spectrum above pH 7.0, contrary to what the bicyclic stabilization model suggests. The data thus do not provide any evidence for a half-protonated state of the CL head group being populated at neutral pH. All the other bands are either pH independent or exhibit only a weak pH-dependence, which indicates minor contributions of PO vibrations to their normal modes.

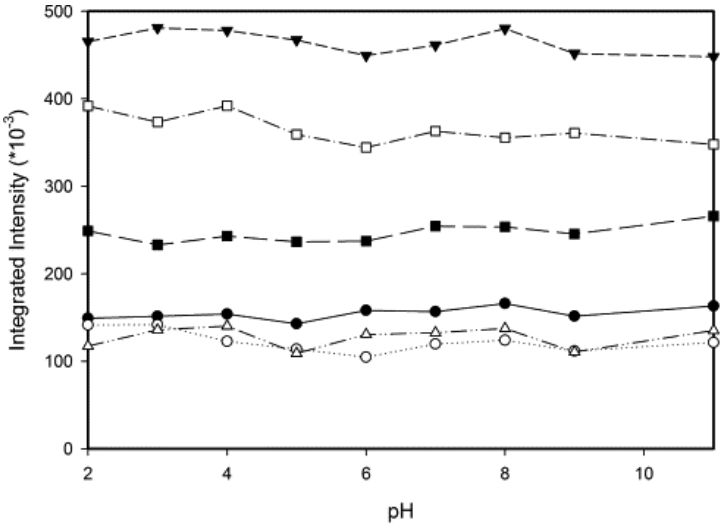

Figure 4.2.2 - Integrated intensity of the bands of the 100% phosphatidylcholine liposomes plotted against the pH. The six bands shown here are centered at 1042 cm^{-1} (black circle),

1060 cm-1 (white circle), 1095 cm^{-1} (black triangle), 1076 cm^{-1} (white triangle), 1218 cm^{-1} (black square), and 1242 cm^{-1} (white square).[115]

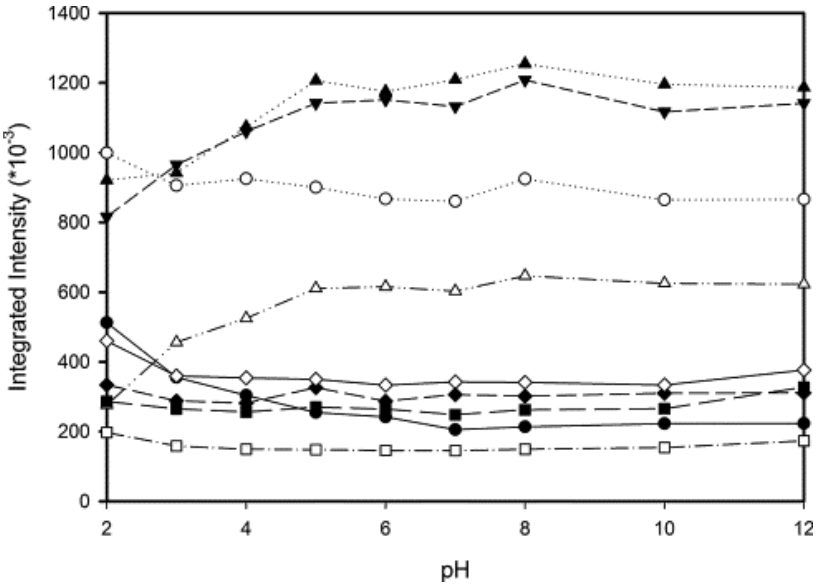

Figure 4.2.3 - Integrated intensity of bands constituting the IR spectrum of 100% cardiolipin liposomes plotted as a function of pH. The band intensities were obtained from a spectral decomposition of spectra measured between 1000 and 1300 cm^{-1}. The bands are labeled as follows: 1017 cm^{-1} (black circle), 1047 cm^{-1} (white circle), 1074 cm^{-1} (black triangle, down), 1094 cm^{-1} (white triangle, up), 1145 cm^{-1} (black square), 1164 cm^{-1} (white square), 1176 cm^{-1} (black diamond), 1193 cm^{-1} (white diamond) and 1214 cm^{-1} (black triangle, up).[115]

The pH-dependence of the TOCL spectrum in the acidic region is further illustrated in Fig. 4.2.4, which displays the difference between the spectrum measured at pH 7 and that measured at the indicated pH. The positive signals in these difference spectra represent the bands whose intensity is reduced toward acidic pH, whereas the negative peaks indicate contribution from the protonated state, which increase with decreasing pH. It makes sense to assign the former to symmetric and antisymmetric combinations of POO^- stretching

modes and the latter to modes of the protonated lipid which involves PO stretching. A more detailed assignment is given based on the normal mode analysis described below.

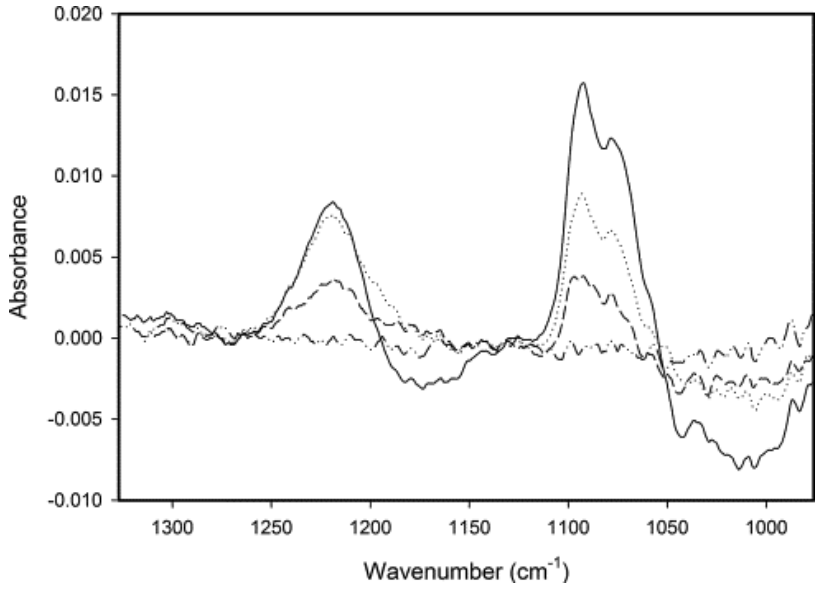

Figure 4.2.4 - Difference infrared spectra across the acidic pH region as compared to neutral pH for 100% cardiolipin liposomes between 1000 and 1300 cm^{-1}. The spectra shown here are obtained by subtracting the spectrum of 100% CL liposomes measured at pH 2 (solid), pH 3 (dotted), pH 4 (dashed), and pH 5 (dashed and dotted) from the spectrum obtained for the same liposomes at neutral pH.[115]

The inner mitochondrial membrane has a mixture of phospholipids, with the cardiolipin concentration standing roughly at 20%. Therefore, the question arises whether liposomes with a 100% CL are truly representative of what one can expect on the surface of the mitochondrial inner membrane. In principle, it can be argued that if mixed protonation states are not obtained on a surface with the high charge density of the 100% TOCL liposomes, one would not expect them to occur if only 20% of the liposome surface is occupied with TOCL. However, since size and curvature of membranes are affected by the

charge distribution, 20% TOCL/80% DOPC liposomes were also checked even though some difficulties discerning the phosphate changes due to low TOCL content were expected. Therefore, IR absorption spectra of 20% TOCL/80% DOPC liposomes were measured as a function of pH in the acidic region. No noticeable spectral changes in pH 4–7 range were observed. At pH 3 and 2, however, the intensity of the high energy part of the low wavenumber band (below 1100 cm^{-1}) decreases, as obtained for 100% TOCL. The underlying bands are assignable to combination of POO^- stretching vibrations to be specified below. Expected spectral changes in the regions below 1050 cm^{-1} and in the region between 1250 and 1300 cm^{-1} seem to be much weaker. However, as indicated in Fig. 4.2.5, spectra changes in the region between 1050 and 1100 cm^{-1} are clearly dominant, so that the difficulty to detect the other changes in the spectra of the 20% TOCL/80% DOPC mixture is not too surprising.

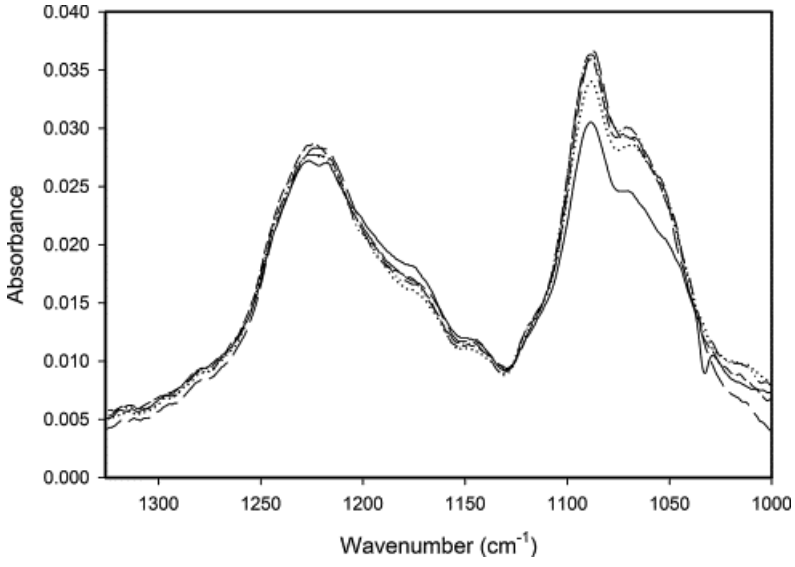

Figure 4.2.5 - FT-IR absorbance spectra of 20% TOCL/80% DOPC liposomes measured at different pH values between 2 and 7. The individual spectra are plotted as follows: pH 2 (solid), pH 3 (dotted), pH 4 (short dash), pH 5 (dashed and dotted), and pH 7 (long dash).[115]

DFT calculations were performed on the head group of the lipid (Fig. 4.2.6) in vacuo on a B3LYP 6-31G** level of theory. After a geometry optimization, a normal mode calculation was carried out. The wavenumbers of all modes obtained were real, indicating that the optimized structure belongs to a minimum of the energy surface. The calculations were carried out with the program TITAN from Schrödinger, Inc. This procedure yielded 28 vibrations in a window between 1000 and 1600 cm^{-1}. Fig. 4.2.7 depicts the spectral density of the vibrational spectrum, i.e., the number of modes in a wavenumber interval of 20 cm^{-1}. Regions containing phosphate group vibrations are marked gray. Most of the modes obtained are more or less delocalized combinations of CH bending, CH_2 and CH_3 deformation modes with some admixtures from CO and CC stretching and OH bending modes. Stretching vibrations of the two phosphate groups are relatively localized. The frequencies of two nearly unmixed antisymmetric OPO stretching modes of the two phosphate groups were obtained as 1307 and 1303 cm^{-1}. There is relatively limited overlap with CH_n deformation modes at the high energy side, while some overlap with non-phosphate group modes is predicted for the low energy side of these two bands. The situation is less clear with regard to the symmetric OPO-stretching vibrations. There are four normal modes between 1090 and 1130 cm^{-1} with admixtures from OPO symmetric stretching vibrations. This region is somewhat separated from a broad spectrum of partially highly delocalized CH_n-deformation modes.

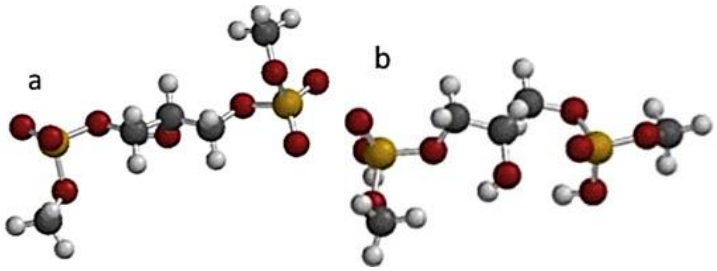

Figure 4.2.6 - Structure of the bi-phosphate head group of ionized (a) and protonated cardiolipin (b) obtained from DFT based geometry optimization. These structures were used to calculate the normal modes discussed in the text. Notice the truncation after the phosphate groups via a methyl group.[115]

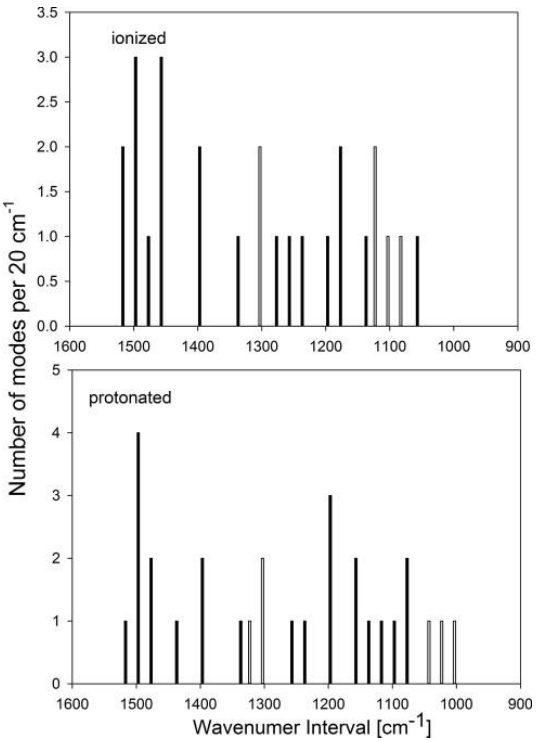

Figure 4.2.7 - Spectral density representation for the frequency interval between 1000 and 1600 cm^{-1} as obtained from the normal mode calculation of the compounds in Fig. 4.2.6. The ordinates display the number of modes obtained in 20 cm^{-1} intervals the lower ends being indicated on the abscissas (1500 cm^{-1} means all modes between 1500 and 1599 cm^{-1} were counted). The upper panel exhibits the mode distribution for the ionized and the lowerpanel the mode distribution for the fully protonated compound. Bars in black

represent combinations of CH deformation and CC stretching modes. Gray bars represent modes with a substantial contributions from PO, PO and CP stretching modes.[115]

A comparison of this normal mode analysis with the decomposed IR spectra suggests that the band at 1213 cm^{-1} results from an overlap of the two barely interacting antisymmetric OPO stretching modes. Bands at lower and higher wavenumbers are assignable to combinations of CH deformation modes. The bands at 1073 and 1094 cm^{-1} should both be related to OPO symmetric stretching modes. The occurrence of two pH dependent bands is in good agreement with the results of normal mode calculations presented here which suggest that OPO symmetric stretch-containing modes are spread over a much larger spectral interval than OPO antisymmetric modes.

DFT and subsequent normal mode calculation for the fully protonated species was also performed, the structure of which is also shown in Fig. 4.2.6. The spectral density distribution is depicted in the lower panel of Fig. 4.2.7. This reveals three modes with contributions from PO stretch at wavenumbers of 1314, 1316 and 1330 cm^{-1}. The PO modes are more delocalized than their counterparts of the fully ionized phosphate groups. The mode exhibiting a frequency of 1314 cm^{-1} is an in-phase and the corresponding mode at 1330 cm^{-1} an out-of-phase combination of the two PO stretching modes. Based on the pH dependence displayed in Fig. 4.2.3, the band at 1192 cm^{-1} is assigned to an overlap of these two modes, from which the out-of-phase combination can be expected to be more intense in an IR spectrum. Thus, band(s) assignable to PO modes were obtained at slightly lower wavenumbers than the bands resulting from antisymmetric POO modes, while the DFT calculations suggest the opposite behavior. To rationalize this discrepancy one has to consider the fact that the wavenumbers of PO stretching modes stretch over a very broad region between 1130 and 1260 cm^{-1}, depending on the chemical environment. The

observed experimental value of 1192 cm^{-1} lies well in this region. On the contrary, the wavenumbers of the asymmetric and symmetric OPO− stretching modes exhibit a much less pronounced variation. The band at 1016 cm^{-1}, the intensity of which increases also with decreasing pH, cannot be assigned to a mode with PO stretching content. The normal mode calculations rather suggest that it should be assigned to a mixture of CH bending and PO, OC and CC stretching vibrations with a normal mode frequency of 1029 cm^{-1}. This band is of course absent in the spectrum of the ionized state of the peptide.

A comparison of calculated and measured frequencies reveals modest scaling factors: 0.9 for POs, 0.92 for the antisymmetric OPO modes, 0.92 for their symmetric counterparts and 0.98 for the PO stretch – OH bending combination.

Thus far, not much effort has been invested into a vibrational analysis of the hydrophilic head group of cardiolipin. Hydrated phosphodiesters usually exhibit bands between 1220 and 1230 cm^{-1} (asymmetric stretch) and 1085–1115 cm^{-1} (symmetric stretch). Hübner et al. measured the IR spectra of 100% cardiolipin and assigned the peak wavenumbers of the broad bands in the 1000–1150 cm^{-1} and 1200–1250 cm^{-1} region to the symmetric (1090 cm^{-1}) and antisymmetric (1215 cm^{-1}) modes.[114] Results presented here suggest that the peak in the 1200 cm^{-1} region is indeed close to the band assignable to the antisymmetric OPO vibration, while a somewhat more nuanced picture emerges for the symmetric stretch combinations, which contributes to several normal modes and therefore covers a broader spectral region. Substantial fractions of the two bands do result from rather delocalized CH-deformation modes. The interference with all types of coupled CH bending and deformation modes as well as CC stretching modes can be expected to be much pronounced in CL than in this truncated model system owing to additional contribution of the lipid

carbon hydrate chains. Some calculations were performed for a larger complex which contained the CL head and the interface between head groups and the carbon hydrate chains at the HF 6-31G** level of theory. They revealed strong overlap between modes of highly coupled CH deformation and e.g., modes with a strong contribution from POO^- antisymmetric stretching. The result explains why the bands that were assigned to stretching modes of the protonated and ionized phosphate groups do not go to zero at neutral (PO) and acidic pH (POO). They either overlap with combinations of CH deformation modes or the phosphate stretching modes constitute just a fraction of the eigenvectors of the modes, which contribute to this spectral region. It should be noted that the pK_a values could not be properly determined due to the instability of the liposomes below the pH of two as well as the inability to isolate any spectral bands that could be solely attributed to the phosphate vibrations rather than vibrations of multiple parts of the molecule.

4.3 – Raman Studies of Ferricytochrome *c* Binding to CL-Containing Membranes

Resonance Raman experiments on oxidized cytochrome c with excitation in the visible region (>400 nm) have been plagued by photoreduction in the past, a known phenomenon with no clear explanation. Alessi et al. showed[84] that photoreduction can also be avoided by oxidizing the protein with potassium ferricyanide and purifying the sample at pH 11.5, when the binding of hexacyanoferrates to lysine side-chains is inhibited, before returning the protein to pH 7.0. The success of their protocol suggests that hexacyanoferrate artifacts in the sample are the electron source for photoreduction. The results of this study led to a

hypothesis that one could actually utilize ferrocyanide-based photoreduction of oxidized cytochrome c to distinguish between native-like and non-native-like proteins attached to CL on liposome surfaces. Because the respective redox potentials are significantly different (220 mV for native like states, −200 mV for non-native states), it seemed likely that photoreduction would only affect native-like conformations that still feature M80 as sixth heme ligand.

As an initial proof of concept, resonance Raman spectra of native oxidized cytochrome *c* in the presence and absence of ferrocyanide in the region between 1300 and 1700 cm^{-1} with 442 nm excitation were recorded. This region contains all the relevant marker bands, that is, ν_4, ν_3, ν_{11}, ν_2, and ν_{10}, which exhibit major changes of their respective wavenumber positions upon a change of the iron's oxidation state (using the notation of Abe et al.). The two spectra are shown in Figure 4.3.1. The protocol of Alessi et al.[84] was used to fully oxidize and purify the protein. After adding ferrocyanide to the protein solution with a stoichiometric ratio of 4:1 at pH 7.0, the observed spectrum indicated practically complete photoreduction. All prominent marker bands in the respective spectrum presented in Figure 4.3.1 showed wavenumber shifts that are diagnostic of a reduction of the heme iron (e.g., from 1374 to 1361 cm^{-1} for the classical oxidation marker ν_4). Therefore, the conclusion is that native oxidized cytochrome c can be photoreduced in the presence of an excess of ferrocyanide.

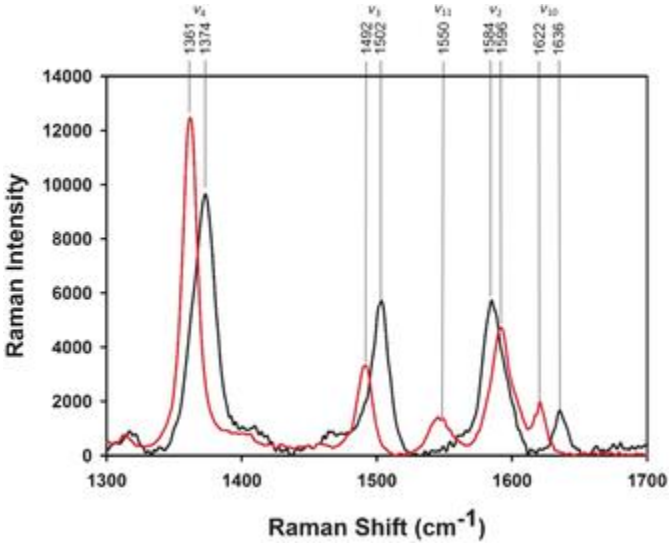

Figure 4.3.1 - Resonance Raman spectrum in the marker band region of non-photoreducible oxidized cytochrome c (black) taken with 442 nm excitation. The accompanying spectrum in red is of the same protein taken the next day in the presence of potassium ferrocyanide at a 4:1 salt to protein molar ratio.[116] The bands are labelled according to band assignments of Abe et al.

Thus, RR spectra of mixtures of 100 μM ferricytochrome c and CL-containing SUVs in the presence of potassium ferrocyanide were measured. Figure 4.3.2 shows the high-frequency RR spectrum of ferricytochrome c obtained with an effective cardiolipin concentration of 500 μM in the outer layers of 20 % TOCL/80 % dioleylphosphocholine DOPC SUVs. This composition was chosen to allow a direct comparison with the spectroscopic data of Pandiscia and Schweitzer-Stenner.[107] The spectrum was decomposed into its individual Lorentzian bands. The band profiles of the canonical marker bands ν_4, ν_3, and ν_{10} showed distinguishable contributions from both oxidation states, proving that the binding of the protein to the liposome surface can at least partially inhibit photoreduction. Because ν_4 is the most intense and isolated oxidation marker band in the spectrum, for which resonance Raman excitation profiles (REPs) of both oxidation states of the protein

have been reported in the literature, it was chosen as a tool for the subsequent quantitative analysis.

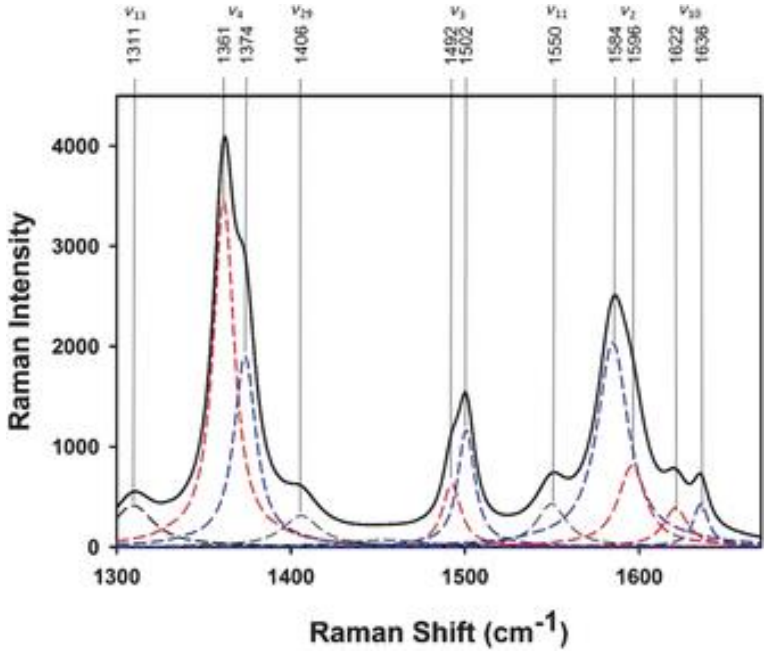

Figure 4.3.2 - High-frequency region of the resonance Raman spectrum of 100 μM (oxidized) cytochrome c in the presence of 20 % DOPC/ 80 % TOCL liposomes (500 μM) and ferrocyanide anions at pH 7.0 taken with 442 nm excitation. Major vibrational bands are labelled according to band assignment of Abe et al. Bands attributable to the reduced and oxidized species are highlighted in red and blue, respectively.[116]

To further explore the relationship between photoreduction and protein binding to CL-containing liposomes, RR spectra of cytochrome c: liposome mixtures as a function of CL concentration were measured. The observed spectra indicated an almost complete inhibition of photoreduction at high lipid concentration, consistent with the predicted predominance of a fraction of non-native proteins. This is clearly demonstrated by difference spectra of the high frequency region in Figure 4.3.3, in which the spectrum of

cytochrome in solution (which is almost entirely in the reduced state due to photoreduction in the presence of ferrocyanide) is subtracted from spectra recorded for the indicated lipid/protein ratio. All spectra were normalized on the structure insensitive ν_{21} band. The use of an internal standard (e.g., sodium perchlorate) is prohibitive because the necessary concentration (0.1 M or higher, if the protein's resonance enhancement is taken into account) would certainly partially inhibit protein binding to the employed SUVs (because of its binding constants of 960 and 310 M^{-1}, the ferrocyanide concentration of 0.4 mM is too low to cause such an undesired side effect). The difference spectra in Figure 4.3.3 display the development of a negative maximum at 1361 cm^{-1} and of a positive maximum at 1374 cm^{-1}, at the position of the ν_4 band for reduced and oxidized species, respectively, which is the clearest indication that photoreduction is being inhibited upon binding to CL-containing SUVs. Both, ν_3 and ν_{10} show similar trends, although a disproportional overall decrease of ν_3 intensity was observed in the oxidized state. Although both ν_2 and ν_{11} also exhibit oxidation-state-dependent changes, the signal-to-noise ratio is insufficient for a quantitative assessment. Of note is an approximately 2 cm^{-1} downshift of the ν_4 of the oxidized protein at high cardiolipin concentration, which can be indicative of a formation of a water-ligated high-spin ferricytochrome c species. Along with pentacoordinate high-spin conformations, such species would be a prime candidate for peroxidase activity, but these assignments cannot be currently confirmed by the appearance of corresponding ν_3 spin-marker band around 1484 and 1492 cm^{-1}.

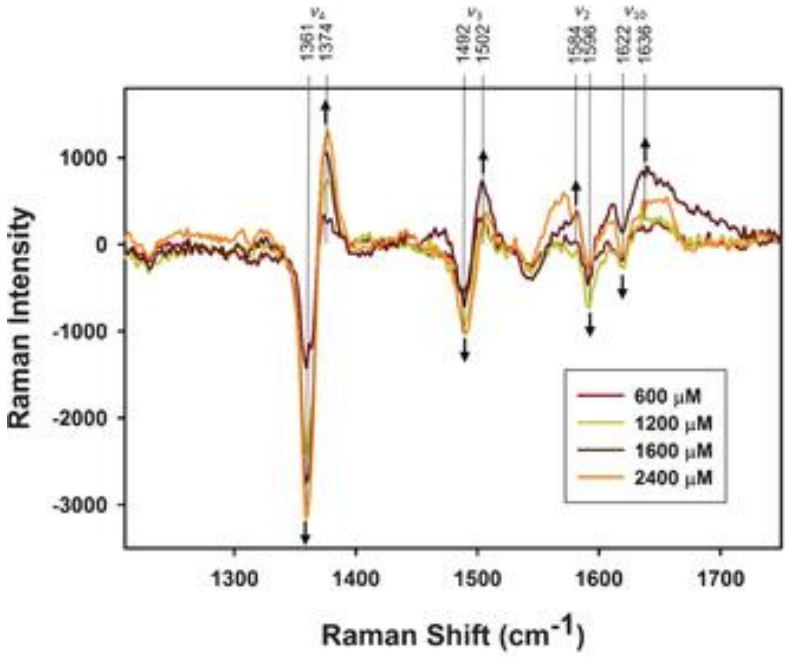

Figure 4.3.3 - Difference spectra in the high-frequency region of resonance Raman spectra of oxidized cytochrome c in the presence of 20% DOPC/80% TOCL SUVs at the indicated CL concentrations, obtained as was described in the text. Positions of major bands are labelled according to band assignments of Abe et al., and arrows indicate the evolution of extrema in the difference spectra for increasing cardiolipin concentrations.[116]

To relate these results to the binding model by Pandiscia and Schweitzer-Stenner,[107] the fraction of the photoreduction-resistant protein was first determined. Taking the intensities of the two sub-bands of the ν_4 allowed a quantitative determination of the fraction of the oxidized species after accounting for the different Raman excitation profiles (see the Experimental Section for details). The thus obtained fraction of oxidized proteins is shown in Figure 4.3.4 as a function of cardiolipin concentration. To explore how these fractions of ferricytochrome c compare with the concentration dependence of the population of the nf- and f-states reported by Pandiscia and Schweitzer-Stenner,[107] the following expression was fitted to the fraction of oxidized state (f_{ox}) data:

$$f_{ox} = \alpha_{nf}\chi_{nf}([CL]) + \alpha_f\chi_f([CL])$$

Where χ_{nf} and χ_f are mole fractions of the nf- and f-states calculated as a function of CL concentration through the global fitting analysis presented by Pandiscia and Schweitzer-Stenner, and α_{nf} and α_f are scaling parameters associated with those mole fractions. In effect, these parameters are fractions of the non-native (i.e. photoreduction-resistant) states in both the nf- and f-states, as these should be the primary states contributing to the photoreduction. The solid line in Figure 4.3.4 shows the results of this fit. The scaling coefficients α_{nf} and α_f obtained from the fit are 0.5 and 1.25, respectively. These values support the assumption that the f state should be the primary contributor to the photoreduction-resistant fraction. Ideally, the value for α_f should be 1. The somewhat higher value might be due to a slight underestimation of the Raman cross-section. If one renormalizes α_f onto 1, one obtains a rescaled value of 0.4 for α_{nf}.

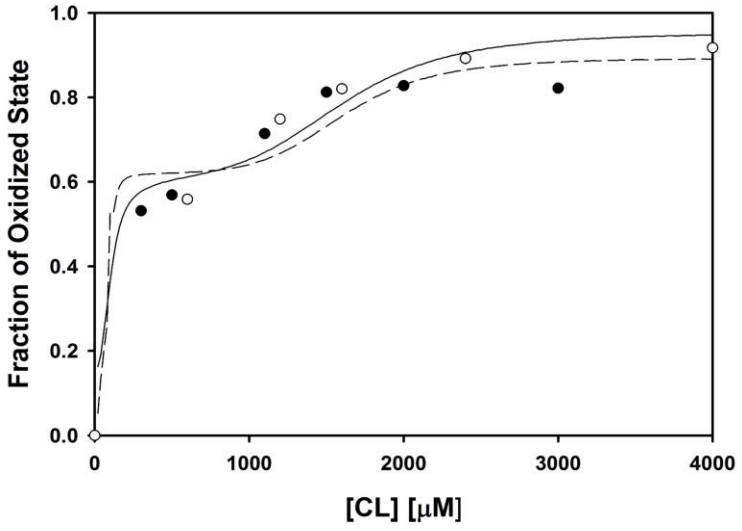

Figure 4.3.4 - Fraction of oxidized cytochrome c plotted as a function of cardiolipin concentration in the outer leaflet of 20 %TOCL/80 %DOPC (open circles) and of 100 % TOCL liposomes (solid circles). The solid and dashed lines result form a fitting procedure described in the text.[116]

To further substantiate the relationship derived above between mole fractions obtained of photoreduced and oxidized species and the populations of the nf and f conformations reported by Pandiscia and Schweitzer-Stenner, Raman spectra of cytochrome c mixed with different amounts of SUVs formed with 100 %TOCL were also recorded and analyzed. A representative Raman spectrum and the corresponding difference spectra are shown in Figures 4.3.5 and 4.3.6.

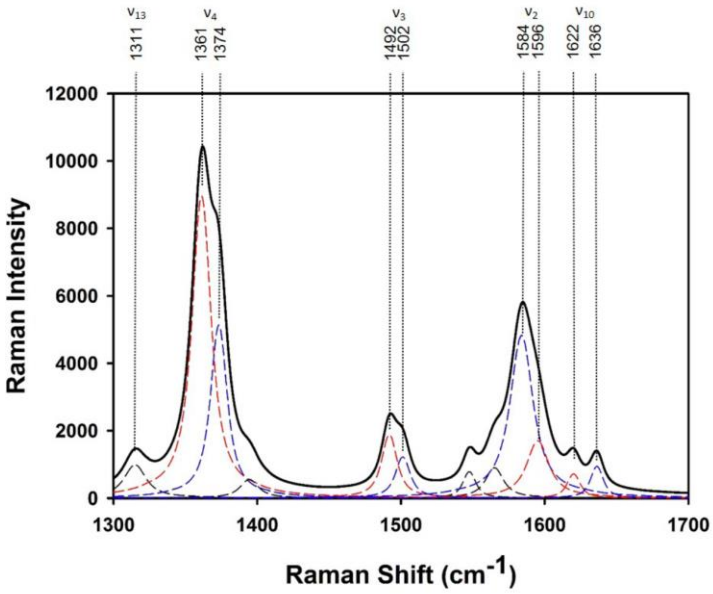

Figure 4.3.5 - High frequency region of the resonance Raman spectrum of a 100 µM solution of oxidized cytochrome c in the presence of 100% TOCL liposomes (500 µM) and ferrocyanide anions taken with 442 nm excitation. Major vibrational bands are labelled according to band assignment of Abe et al. Bands attributable to the reduced and oxidized species are highlighted in red and blue, respectively.[116]

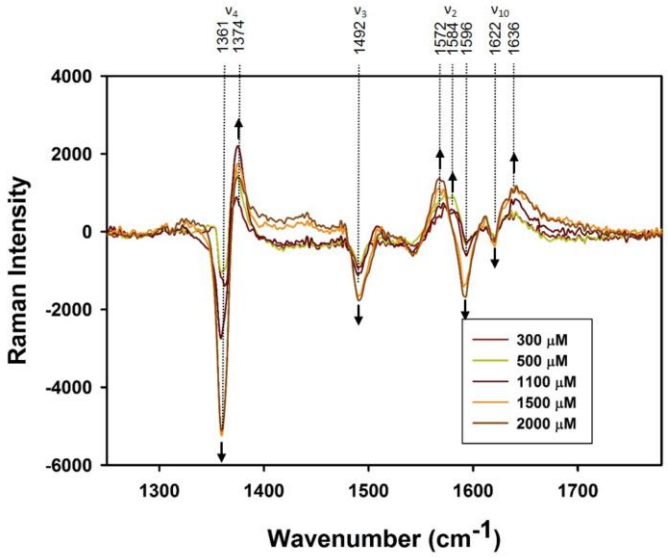

Figure 4.3.6 - Difference spectra in the high frequency region of resonance Raman spectra of oxidized cytochrome c in the presence of 100% TOCL SUVs at the indicated CL concentrations, obtained as described in the text. Positions of major bands are labelled according to band assignments of Abe et al., and arrows indicate the evolution of extrema in the difference spectra for increasing cardiolipin concentrations.[116]

Because the range of CL concentration of the experiment was the same as that used for 20%TOCL/80%DOPC, the overall binding affinity increased due to an increase of the protein density on the liposome surface. At high lipid concentrations, the f/nf ratio is slightly lower for cytochromes bound to 100% TOCL liposomes. The nf- and f-fractions were again calculated for the CL and protein concentrations used for the Raman experiments and scaled them to the respective fraction of oxidized proteins observed from the analysis of the ν_4 band (open circles in Figure 4.3.4). This gave the same α_{nf} and α_f values (i.e., 0.5 and 1.25) that were used to fit the data for 20%TOCL/80%DOPC.

Based on the analysis described above, one can conclude that 60 % of the nf conformers are photoreduced and must therefore be considered as a native state. As was stated earlier, the nf(C) ensemble should be considered as a heterogeneous mixture of native-like and very compact non-native-like states. It needs to be emphasized that owing to the uncertainties associated with equilibrium constant for the nf/f distribution at low CL concentrations (ca. 30 %), the α_{nf} is subject to larger statistical errors.

These results underscore the notion that the earlier obtained conformations nf and f (or C and E) represent heterogeneous conformational sub-ensembles. They further suggest that a substantial fraction of the nf/C sub-ensemble exhibits a native-like conformation with M80 as the sixth ligand. The remaining fraction of this sub-ensemble is likely to be in some type of molten globule state.

4.4 – Binding at Slightly Acidic pH as Probed by Raman Spectroscopy

Measurements of the binding at slightly acidic pH are of particular interest for multiple reasons. First, Nantes' L-site binding is expected to compete with A-site binding that Kinnunen and co-workers have proposed.[94] Furthermore, at least one of the histidine ligands that can possibly replace the native methionine upon CL-induced unfolding is expected to be protonated. If any particular differences in binding are observed in this pH regime, they are most likely attributable to the protonation of this histidine. Hence, the binding was first probed via fluorescence, circular dichroism, and UV/Visible absorption spectroscopies by Milorey, with the data indicating that there are quite a few observable differences in binding. A particularly interesting finding, however, was a conversion to a

high-spin state, something clearly not observed for binding at pH 7.4 (i.e. the pH Pandiscia's experiments were performed at).

To gain further insights into structural changes caused by cytochrome *c* binding to CL liposomes at acidic pH, resonance Raman (RR) spectra of different cytochrome–liposome mixtures were measured at pH 6.5. The difference spectra for these data set are shown in Figure 4.4.1.

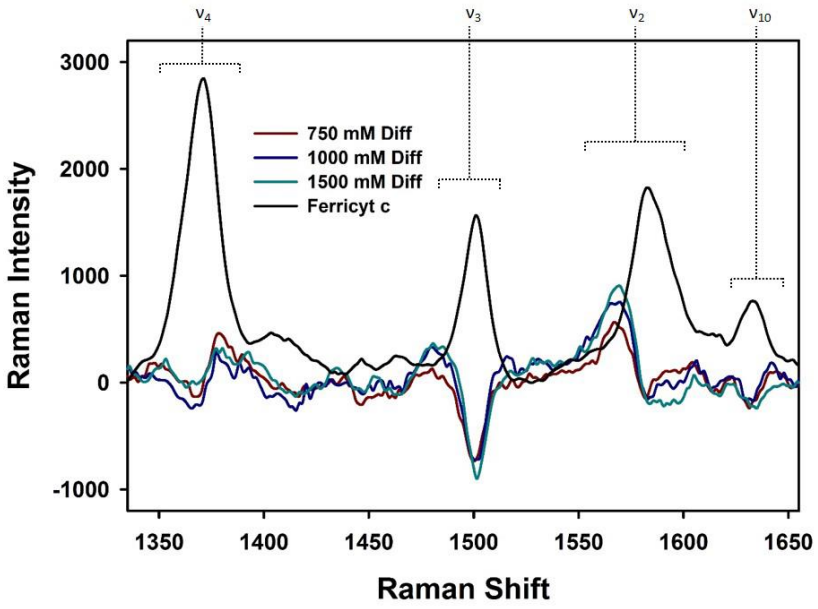

Figure 4.4.1 - Difference spectra for ferricytochrome c – CL liposome systems, where the spectrum of ferricytochrome c in solution (shown in black for scale) is subtracted from the spectrum obtained for the protein with CL at the indicated concentrations. Of note is a clear contribution of a blueshifted ν_4 band, most likely assignable of bis-His species that is also described in the text, and a clear increase in intensity of the high-spin components of the ν_3 and ν_2.[117]

A rapid loss of the low-spin component of the ν_3 intensity with increasing CL concentrations and a concomitant gain in intensity of specific high-spin components of multiple spin marker bands (ν_2, ν_3, and ν_{10}) was observed, as revealed by the deconvolution of the RR spectrum measured in the presence of 1500 μM CL. This deconvolution is shown in Figure 4.4.2 below.

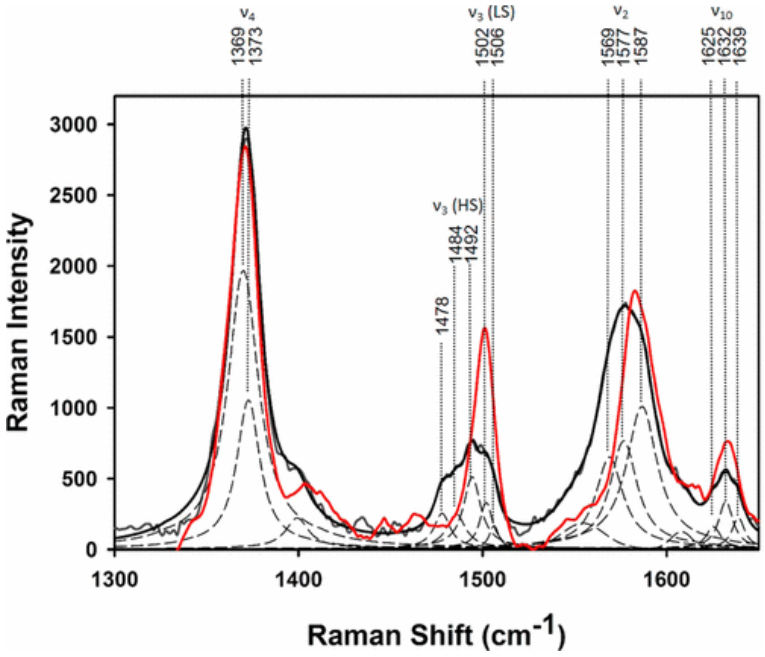

Figure 4.4.2 - Resonance Raman spectrum of a pH 6.5 50 μM ferricytochrome *c* solution at a cardiolipin concentration of 0 μM (red) and 1500 μM (gray) as obtained with 442 nm excitation, shown along with the decomposition (dashed black) and the total fit (solid black) of the latter spectrum.[117] Sub-bands are labeled according to the notation of Abe et al.

Each spin marker band has at least three components that were required to fit all of the spectra consistently, indicative of the coexistence of at least three species. For the ν_3 band, the specific sub-bands at 1485 and 1492 cm^{-1} are dominant; the two sub-bands above 1500

cm^{-1} contribute very little to the band profile. By taking into account the lower resonance enhancement expected for the high-spin species in comparison with their low-spin counterparts due to the blue shift of the Soret maximum, an estimated ~10% of the protein is still in a low-spin configuration. On the basis of the assignments reported by Oellerich et al.,[50] the sub-bands at 1485 and 1492 cm^{-1} are indicative of pentacoordinated and water-ligated hexacoordinated high-spin species, respectively. These assignments are further corroborated by the appearance of ν_2 sub-bands at 1569 and 1577 cm^{-1}, respectively, and a ν_{10} sub-band at 1625 cm^{-1}. The low-spin sub-bands reflect some residual deprotonated bis-His species. The bis-His assignment is corroborated by the observed ν_4, ν_3, and ν_{10} components found at 1373, 1502, and 1639 cm^{-1}, respectively. It is of note that a weak "ν_3" sub-band at 1478 cm^{-1} was observed, and there is no current assignment available in the literature.

The RR spectra of ferricytochrome *c* at a high CL concentration and 150 mM NaCl in the absence and presence of ferrocyanide are shown in Figure 4.4.3. In the absence of ferrocyanide, the spectrum resembles that of a native (or native-like) ferricytochrome *c* system. Upon the addition of ferrocyanide, the spectrum reveals complete photoreduction, which indicates that in the presence of salt ferricytochrome *c* exists in its native conformation even at high CL concentrations. This observation corroborates the notion that the binding of cytochrome *c* to CL liposomes observed at pH 6.5 is entirely electrostatic in nature. Note that the spectral noise is high due to reduced collection time.

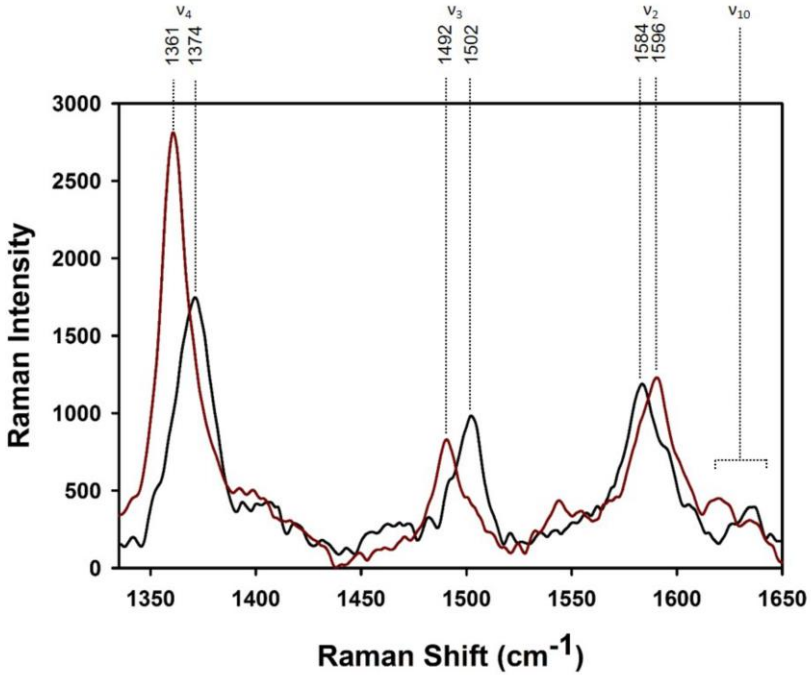

Figure 4.4.3 - Resonance Raman spectra of ferricytochrome c in the presence of 2000 μM CL and 150 μM NaCl, both in the absence (black) and presence (red) of ferrocyanide in a 1:12 protein to ferrocyanide ratio. Note the complete photoreduction, as indicated by the oxidation marker bands, after the addition of salt.[117]

Taken together, the data suggest a reversible electrostatically driven binding of ferricytochrome *c* to CL membranes at mildly acidic pH that is reminiscent of the previously proposed L-site binding mode, with clear evidence for a predominance of a high spin state.

4.5 – Discussion of Results

4.5.1 - Summary

A vibrational spectroscopic approach in studying the cytochrome *c* – CL system has been presented. Infrared spectroscopy has been used to specifically look at TOCL (and DOPC) phosphate vibrations as a function of pH (section 4.2). DOPC liposomes' infrared spectra show little to no pH dependence, indicating that they are truly neutral (zwitterionic) across

the tested pH range and can serve as a well-behaving background lipid. TOCL spectra also show no pH dependence over the alkaline region, thus casting doubt on the bicyclic stabilization model of Kates et al. that suggests a $pK_{a,2}$ between pH 7.5 and 9.5.[59] However, the situation is different in the acidic region. Here, distinct spectral changes were detected that were attributed to changes in protonation states. Decomposition of the spectra reveal a rather dense spectral region, and the subsequent tracking of infrared band intensities over the pH range of bands attributable to PO vibrations showed that they did not lose all of their intensity upon deprotonation and nor did bands attributable to OPO^-, as would be expected in a perfect system. While it can be argued that the latter effect is likely due to one group still existing in a deprotonated state and thus contributing POO^- related bands to the spectrum before $pK_{a,1}$ is reached, the former is hard to explain without DFT calculations. DFT calculations performed on a model system consisting of a truncated CL headgroup (where the glycerol of each dioleyl phosphatidic acid was simply replaced with a methyl group) revealed a high degree of coupling between CH_n deformation modes with phosphate vibrational modes, with this being the likely explanation as to why there is no full disappearance of vibrational bands assignable to PO vibrations even after deprotonation to OPO^-.

The applications of resonance Raman spectroscopy in studying this system were also explored. A classical tool in the study of heme proteins, resonance Raman has been thus far underutilized to study this system, most likely due to the experimental difficulties associated with the introduction of liposomes into the system and photoreduction. In section 4.3, however, photoreduction was presented as an actual tool rather than a detriment in studying this system, with the data indicating that CL can inhibit photoreduction by

inducing structural changes in the protein that cause it to lose its redox potential-mediating methionine ligand. The fraction of the oxidized state was calculated at each CL concentration by the decomposition of the spectra and the adjustment to the REPs. Through tracking of the non-photoreduceable fraction as a function of CL concentration and the assignment of this fraction as a contribution of both the nf- and f-states (with the latter expected to be the dominant contributor) of the Pandiscia model, the data for two different set of liposomes (20% CL and 100% CL) was fit with the calculated fractions of these two states via weighting parameters. These weighting parameters indicated that approximately 40% of the nf-state and 100% of the f-state contributes to the photoreduction-resistant fraction, as expected.

In section 4.4, it is shown how resonance Raman can be applied to studying the binding at acidic pH, where L-site binding is expected to be active and one of the histidine ligands (that can serve as a possible replacement of the methionine ligand) is protonated. First, marker bands of the resonance Raman spectra in the high frequency region show that a large fraction of the protein adopts a high spin configuration, and that this high spin population consists of pentacoordinated and hexacoordinated high spin species. This is a clear departure from the dominant low-spin population observed during binding at neutral pH, indicating that there is a new mode of binding. Furthermore, it was shown through the photoreduction method that this binding is purely electrostatic, where the bound protein - that was shown to be completely photoreduction resistant – regains its ability to photoreduce after the addition of salt, indicative of the repopulation of a native-like state.

4.5.2 – Discussion and Significance of Results

The infrared results, specifically the lack of pH dependence observed for the infrared spectra of CL-containing liposomes above pH of 7.0, serve to solve the discrepancy regarding the ionization state of CL. These results show that the bicyclic stabilization of the monoionized state model of Kates et al.[118] that proposed a $pK_{a,2}$ between 7.5 and 9.5 is incorrect, rather supporting the doubly ionized model. It should be noted here that more recent work[119] has supported the doubly ionized view, as well. An ionization state of -2 allows for a much stronger electrostatic interaction between cytochrome *c* and CL while giving a greater charge density to CL-containing membranes. A pH dependence was only observed below the pH of 5.0, i.e. the pH where Kinnunen and co-workers first saw C-site binding.[94] This links the appearance of the new binding site to the protonation of CL, though no direct connection has been established through these studies. As stated above, this study also served as one of the first full analyses of the CL phosphate headgroup vibrational spectra, revealing the high degree of complexity in a relatively small frequency region.

Photoreduction being presented as a tool is in itself quite novel, as it is a very classical and well-documented problem in the studying of the oxidized versions of heme proteins. However, here it is clearly shown that photoreduction can be used to study the binding of cytochrome *c* to cardiolipin membranes due to the drop in the redox potential caused by the dissociation of the native methionine ligand. This redox potential drop and the accompanying inhibition of photoreduction allow the direct tracking of all non-native-like conformations, i.e. conformations lacking the M80 ligation. In effect, measurement of RR spectra in the presence of ferrocyanide can be used to isolate the CL-bound conformations

from the unbound ones, where the fraction of the protein that is unbound experiences complete photoreduction and becomes spectroscopically isolated due to the marked changes in the marker bands upon change in oxidation state. It should be noted that such an approach would not account for 60% of the bound nf-state that was shown to remain in the native-like conformation. This shows that photoreduction can be used as a very powerful tool for studying binding of cytochrome *c* to charged membranes.

Lastly, binding at slightly acidic pH is highly relevant due to the expected pH of the mitochondria being approximately 6.9 (with possibly lower pH values on the surface of the negatively charged membrane due to accumulation of protons). It is around pH 6.5 that the L-site binding described by Nantes and coworkers[97] becomes active. There is clear evidence that the protein mostly adopts high-spin conformations of the penta- and hexacoordinated type upon binding to CL-containing membranes at neutral pH. These conformations are of particular interest because they would be expected to contribute to the observed peroxidase activity, with the pentacoordinated high-spin state expected to be the primary contributor. Furthermore, the binding at this pH was shown to be electrostatic in nature through salt experiments, fully consistent with L-site binding. The question as to what ligand replaces the M80 has been outstanding for a while, with evidence presented in favor of either a histidine ligand or a lysine ligand. Due to the observed changes occurring in the pH regime where a histidine residue becomes protonated, these observed changes in the binding mode are thus indicative that histidine is responsible for replacing the native M80 during CL-induced unfolding.

CHAPTER 5 – SUMMARY AND OUTLOOK

While cytochrome *c* involvement in apoptosis has now been studied for many years, some issues are still poorly understood regarding its specific interaction with cardiolipin. It is clear that the protein can bind to the CL-containing membranes in many ways from the different binding sites proposed by Kinnunen and coworkers (A and C sites) as well as Nantes and coworkers (L site). Furthermore, it is evident that the protein exhibits an equilibrium on the surface of CL-containing liposomes, with Pletneva and coworkers describing it as an equilibrium between a compact and an extended state while Pandiscia and Schweitzer-Stenner proposed a model where cytochrome *c* binding experiences a CL-dependent equilibrium between a native-like nf- state and a non-native f-state. These states are reminiscent of those proposed by Pletneva and coworkers, but their exact structural conformations are still unknown.

While many studies describing the binding have now been published, an unresolved issue in the field focusing on the ionization state of cardiolipin still stands. Kates et al. described a bicyclic structure that stabilized the monoionized version of CL well into the basic region, meaning that the lipid exhibits a -1 charge at neutral pH. However, this is at odds with many traditional titration experiments that suggest that CL carries a -2 charge. To resolve this issue, infrared spectroscopy analysis of the phosphate headgroups was presented in this thesis. Based on the pH dependence of the different bands occurring only in the pH 2-5 region, it is clear that CL is doubly-ionized at neutral pH. Furthermore, DFT calculations aided in the assignments of the different bands, clarifying the rather complex phosphate vibrational region in the infrared spectrum. Now, with the resolution of this issue presented here, the interaction between cytochrome *c* and CL is clearer. The C-site binding of

Kinnunen and coworkers was observed to become active below pH 5, which is clearly the region where CL becomes protonated.

Another vibrational technique that has seen rare use in studying this system is resonance Raman. It is rather peculiar to observe this lack of use, simply due to the power of resonance Raman in studying heme proteins. The structural analysis of the different conformers on the surface of the membrane is still outstanding, as has been mentioned. This thesis has presented a new technique that can be used to study the binding – specifically, photoreduction was turned into a powerful tool through which it was possible to track the bound non-native conformers of the protein. The results are in good agreement with the Pandiscia and Schweitzer-Stenner binding model for two different sets of liposomes, implying that this is a powerful technique that can be used as a complement to other spectroscopic analyses.

It is still not clear what ligand replaces the native methionine 80 during CL-induced unfolding, with both histidines and lysines being possible candidates. Measuring the binding at slightly acidic pH is an attractive option due to the fact that one of the histidines that can possibly replace M80 is now protonated. Furthermore, L-site binding can start to compete with A-site binding all while these experiments are biologically relevant due to the slightly acidic mitochondrial pH. Resonance Raman measurements on this system quickly showed that there is dominance of high-spin ferricytochrome *c* species, both of the pentacoordinated and hexacoordinated (water-ligated) variety. These states are expected to be the primary contributors to peroxidase activity of the protein that is required for its function as a pro-apoptotic factor. Furthermore, the fact that there is such a drastic

difference in binding upon protonation of histidine implies that histidine is responsible for replacing M80 upon binding at neutral pH.

BIBLIOGRAPHY

1. Wright, P. E.; Dyson, H. J., Intrinsically Disordered Proteins in Cellular Signaling and Regulation. *Nature reviews. Molecular cell biology* **2015**, *16*, 18-29.
2. Dyson, H. J.; Wright, P. E., Intrinsically Unstructured Proteins and Their Functions. *Nat Rev Mol Cell Biol* **2005**, *6*, 197-208.
3. Atlante, A.; Calissano, P.; Bobba, A.; Azzariti, A.; Marra, E.; Passarella, S., Cytochrome C Is Released from Mitochondria in a Reactive Oxygen Species (Ros)-Dependent Fashion and Can Operate as a Ros Scavenger and as a Respiratory Substrate in Cerebellar Neurons Undergoing Excitotoxic Death. *The Journal of biological chemistry* **2000**, *275*, 37159-66.
4. Hashimoto, M.; Takeda, A.; Hsu, L. J.; Takenouchi, T.; Masliah, E., Role of Cytochrome C as a Stimulator of Alpha-Synuclein Aggregation in Lewy Body Disease. *The Journal of biological chemistry* **1999**, *274*, 28849-52.
5. Branden, C. I. T., J., *Introduction to Protein Structure*; Garland Science, 1999.
6. Nelson, D. L. C., M. M., *Lehninger Principles of Biochemistry*, 6th ed., 2013.
7. Sela, M.; White, F. H., Jr.; Anfinsen, C. B., Reductive Cleavage of Disulfide Bridges in Ribonuclease. *Science (New York, N.Y.)* **1957**, *125*, 691-2.
8. Levinthal, C., Are There Pathways for Protein Folding? *J. Chim. Phys.* **1968**, *65*, 44-45.
9. Kauzmann, W., Some Factors in the Interpretation of Protein Denaturation. *Advances in protein chemistry* **1959**, *14*, 1-63.
10. Onuchic, J. N.; Socci, N. D.; Luthey-Schulten, Z.; Wolynes, P. G., Protein Folding Funnels: The Nature of the Transition State Ensemble. *Folding and Design* **1996**, *1*, 441-450.
11. Soffer, J. B.; Fradkin, E.; Pandiscia, L. A.; Schweitzer-Stenner, R., The (Not Completely Irreversible) Population of a Misfolded State of Cytochrome C under Folding Conditions. *Biochemistry* **2013**, *52*, 1397-1408.
12. Hartl, F. U.; Hayer-Hartl, M., Converging Concepts of Protein Folding in Vitro and in Vivo. *Nature structural & molecular biology* **2009**, *16*, 574-81.
13. Jaenicke, R., Protein Structure and Function at Low Temperatures. *Philosophical transactions of the Royal Society of London. Series B, Biological sciences* **1990**, *326*, 535-51; discussion 551-3.
14. de Kruijff, B.; Cullis, P. R., Cytochrome C Specifically Induces Non-Bilayer Structures in Cardiolipin-Containing Model Membranes. *Biochimica et Biophysica Acta (BBA) - Biomembranes* **1980**, *602*, 477-490.
15. Kinnunen, P. K., Fusion of Lipid Bilayers: A Model Involving Mechanistic Connection to Hii Phase Forming Lipids. *Chemistry and physics of lipids* **1992**, *63*, 251-8.
16. Perera, Meenu N.; Lin, Shang H.; Peterson, Yuri K.; Bielawska, A.; Szulc, Zdzislaw M.; Bittman, R.; Colombini, M., Bax and Bcl-Xl Exert Their Regulation on Different Sites of the Ceramide Channel. *Biochemical Journal* **2012**, *445*, 81-91.
17. Singer, S. J., The Molecular Organization of Membranes. *Annual review of biochemistry* **1974**, *43*, 805-33.
18. Simons, K.; Ikonen, E., Functional Rafts in Cell Membranes. *Nature* **1997**, *387*, 569-572.
19. Hartmann, W.; Galla, H. J., Binding of Polylysine to Charged Bilayer Membranes: Molecular Organization of a Lipid.Peptide Complex. *Biochimica et biophysica acta* **1978**, *509*, 474-90.
20. Iwai, A.; Masliah, E.; Yoshimoto, M.; Ge, N.; Flanagan, L.; de Silva, H. A.; Kittel, A.; Saitoh, T., The Precursor Protein of Non-a Beta Component of Alzheimer's Disease Amyloid Is a Presynaptic Protein of the Central Nervous System. *Neuron* **1995**, *14*, 467-75.
21. Zhao, M.; Cascio, D.; Sawaya, M. R.; Eisenberg, D., Structures of Segments of Alpha-Synuclein Fused to Maltose-Binding Protein Suggest Intermediate States During Amyloid Formation. *Protein science : a publication of the Protein Society* **2011**, *20*, 996-1004.

22. Spillantini, M. G.; Crowther, R. A.; Jakes, R.; Hasegawa, M.; Goedert, M., Alpha-Synuclein in Filamentous Inclusions of Lewy Bodies from Parkinson's Disease and Dementia with Lewy Bodies. *Proceedings of the National Academy of Sciences of the United States of America* **1998**, *95*, 6469-73.
23. Yu, C.; Lou, J.; Wu, J.; Pan, L.; Feng, W.; Zhang, M., Membrane-Induced Lever Arm Expansion Allows Myosin Vi to Walk with Large and Variable Step Sizes. *The Journal of biological chemistry* **2012**, *287*, 35021-35035.
24. Bushnell, G. W.; Louie, G. V.; Brayer, G. D., High-Resolution Three-Dimensional Structure of Horse Heart Cytochrome C. *Journal of molecular biology* **1990**, *214*, 585-95.
25. Goldbeck, R. A.; Chen, E.; Kliger, D. S., Early Events, Kinetic Intermediates and the Mechanism of Protein Folding in Cytochrome C. *International journal of molecular sciences* **2009**, *10*, 1476-99.
26. Takano, T.; Dickerson, R. E., Conformation Change of Cytochrome C. I. Ferrocytochrome C Structure Refined at 1.5 a Resolution. *Journal of molecular biology* **1981**, *153*, 79-94.
27. Pande, A.; Myer, Y. P., The Redox Potential of Horse Heart Cytochrome C. *Biochemical and Biophysical Research Communications* **1978**, *85*, 7-13.
28. Larsen, D. Transition Metals in Biology. (accessed June 2).
29. Shah, R.; Schweitzer-Stenner, R., Structural Changes of Horse Heart Ferricytochrome C Induced by Changes of Ionic Strength and Anion Binding. *Biochemistry* **2008**, *47*, 5250-7.
30. Trewhella, J.; Carlson, V. A.; Curtis, E. H.; Heidorn, D. B., Differences in the Solution Structures of Oxidized and Reduced Cytochrome C Measured by Small-Angle X-Ray Scattering. *Biochemistry* **1988**, *27*, 1121-5.
31. Liu, G. Y.; Grygon, C. A.; Spiro, T. G., Ionic Strength Dependence of Cytochrome C Structure and Trp-59 H/D Exchange from Ultraviolet Resonance Raman Spectroscopy. *Biochemistry* **1989**, *28*, 5046-50.
32. Connolly, M. L., Solvent-Accessible Surfaces of Proteins and Nucleic Acids. *Science (New York, N.Y.)* **1983**, *221*, 709-13.
33. Shelnutt, J. A.; Rousseau, D. L.; Dethmers, J. K.; Margoliashi, E., Protein Influence on the Heme in Cytochrome C: Evidence from Raman Difference Spectroscopy. *Proceedings of the National Academy of Sciences* **1979**, *76*, 3865-3869.
34. Jentzen, W.; Song, X.-Z.; Shelnutt, J. A., Structural Characterization of Synthetic and Protein-Bound Porphyrins in Terms of the Lowest-Frequency Normal Coordinates of the Macrocycle. *The Journal of Physical Chemistry B* **1997**, *101*, 1684-1699.
35. Liptak, M. D.; Wen, X.; Bren, K. L., Nmr and Dft Investigation of Heme Ruffling: Functional Implications for Cytochrome C. *Journal of the American Chemical Society* **2010**, *132*, 9753-9763.
36. Dickerson, R. E.; Takano, T.; Eisenberg, D.; Kallai, O. B.; Samson, L.; Cooper, A.; Margoliash, E., Ferricytochrome C. I. General Features of the Horse and Bonito Proteins at 2.8 a Resolution. *The Journal of biological chemistry* **1971**, *246*, 1511-35.
37. Filosa, A.; Wang, Y.; Ismail, A. A.; English, A. M., Two-Dimensional Infrared Correlation Spectroscopy as a Probe of Sequential Events in the Thermal Unfolding of Cytochromes C. *Biochemistry* **2001**, *40*, 8256-63.
38. Porcelli, A. M.; Ghelli, A.; Zanna, C.; Pinton, P.; Rizzuto, R.; Rugolo, M., Ph Difference across the Outer Mitochondrial Membrane Measured with a Green Fluorescent Protein Mutant. *Biochem Biophys Res Commun* **2005**, *326*, 799-804.
39. Wallace, C. J.; Clark-Lewis, I., Functional Role of Heme Ligation in Cytochrome C. Effects of Replacement of Methionine 80 with Natural and Non-Natural Residues by Semisynthesis. *Journal of Biological Chemistry* **1992**, *267*, 3852-3861.
40. Ow, Y. P.; Green, D. R.; Hao, Z.; Mak, T. W., Cytochrome C: Functions Beyond Respiration. *Nat Rev Mol Cell Biol* **2008**, *9*, 532-42.

41. Theorell, H.; Åkesson, Å., Studies on Cytochrome C. Iii. Titration Curves. *Journal of the American Chemical Society* **1941**, *63*, 1818-1820.
42. Yeh, S. R.; Takahashi, S.; Fan, B.; Rousseau, D. L., Ligand Exchange During Cytochrome C Folding. *Nature structural biology* **1997**, *4*, 51-6.
43. Yeh, S.-R.; Rousseau, D. L., Ligand Exchange During Unfolding of Cytochrome C. *Journal of Biological Chemistry* **1999**, *274*, 17853-17859.
44. Colón, W.; Elöve, G. A.; Wakem, L. P.; Sherman, F.; Roder, H., Side Chain Packing of the N- and C-Terminal Helices Plays a Critical Role in the Kinetics of Cytochrome C Folding. *Biochemistry* **1996**, *35*, 5538-5549.
45. Indiani, C.; de Sanctis, G.; Neri, F.; Santos, H.; Smulevich, G.; Coletta, M., Effect of Ph on Axial Ligand Coordination of Cytochrome C" from Methylophilus Methylotrophus and Horse Heart Cytochrome C. *Biochemistry* **2000**, *39*, 8234-42.
46. Dyson, H. J.; Beattie, J. K., Spin State and Unfolding Equilibria of Ferricytochrome C in Acidic Solutions. *The Journal of biological chemistry* **1982**, *257*, 2267-73.
47. Assfalg, M.; Bertini, I.; Dolfi, A.; Turano, P.; Mauk, A. G.; Rosell, F. I.; Gray, H. B., Structural Model for an Alkaline Form of Ferricytochrome C. *J Am Chem Soc* **2003**, *125*, 2913-22.
48. Döpner, S.; Hildebrandt, P.; Rosell, F. I.; Mauk, A. G., Alkaline Conformational Transitions of Ferricytochrome C Studied by Resonance Raman Spectroscopy. *Journal of the American Chemical Society* **1998**, *120*, 11246-11255.
49. Pandiscia, L. A. Conformational Diversity of Cytochrome *C* on Cardiolipin - Containing Liposomes Probed by Optical Spectroscopy. Drexel University, Philadelphia, PA, 2015.
50. Oellerich, S.; Wackerbarth, H.; Hildebrandt, P., Spectroscopic Characterization of Nonnative Conformational States of Cytochrome C. *J. Phys. Chem. B.* **2002**, *106*, 6566-6580.
51. Verbaro, D.; Hagarman, A.; Soffer, J.; Schweitzer-Stenner, R., The Ph Dependence of the 695 Nm Charge Transfer Band Reveals the Population of an Intermediate State of the Alkaline Transition of Ferricytochrome C at Low Ion Concentrations. *Biochemistry* **2009**, *48*, 2990-6.
52. Finnegan, M. L.; Bowler, B. E., Propensities of Aromatic Amino Acids Versus Leucine and Proline to Induce Residual Structure in the Denatured-State Ensemble of Iso-1-Cytochrome C. *Journal of molecular biology* **2010**, *403*, 495-504.
53. Weinkam, P.; Zimmermann, J.; Sagle, L. B.; Matsuda, S.; Dawson, P. E.; Wolynes, P. G.; Romesberg, F. E., Characterization of Alkaline Transitions in Ferricytochrome C Using Carbon–Deuterium Infrared Probes. *Biochemistry* **2008**, *47*, 13470-13480.
54. Krishna, M. M.; Lin, Y.; Mayne, L.; Englander, S. W., Intimate View of a Kinetic Protein Folding Intermediate: Residue-Resolved Structure, Interactions, Stability, Folding and Unfolding Rates, Homogeneity. *Journal of molecular biology* **2003**, *334*, 501-13.
55. Maity, H.; Maity, M.; Krishna, M. M. G.; Mayne, L.; Englander, S. W., Protein Folding: The Stepwise Assembly of Foldon Units. *Proceedings of the National Academy of Sciences of the United States of America* **2005**, *102*, 4741-4746.
56. Cortese, J. D.; Voglino, A. L.; Hackenbrock, C. R., Multiple Conformations of Physiological Membrane-Bound Cytochrome C. *Biochemistry* **1998**, *37*, 6402-6409.
57. Wang, X., The Expanding Role of Mitochondria in Apoptosis. *Genes & development* **2001**, *15*, 2922-33.
58. Kagan, V. E.; Borisenko, G. G.; Tyurina, Y. Y.; Tyurin, V. A.; Jiang, J.; Potapovich, A. I.; Kini, V.; Amoscato, A. A.; Fujii, Y., Oxidative Lipidomics of Apoptosis: Redox Catalytic Interactions of Cytochrome C with Cardiolipin and Phosphatidylserine. *Free radical biology & medicine* **2004**, *37*, 1963-85.
59. Kates, M.; Syz, J.-Y.; Gosser, D.; Haines, T. H., Ph-Dissociation Characteristics of Cardiolipin and Its 2′-Deoxy Analogue. *Lipids* **1993**, *28*, 877-882.

60. Lemmin, T.; Bovigny, C.; Lançon, D.; Dal Peraro, M., Cardiolipin Models for Molecular Simulations of Bacterial and Mitochondrial Membranes. *Journal of Chemical Theory and Computation* **2013**, *9*, 670-678.
61. Coulon-Morelec, M. J.; Faure, M.; Marechal, J., [Controlled Degradation of Diphosphatidylglycerol (Cardiolipid) in an Acid Medium. Study of the Phosphatide Derivatives Obtained]. *Bulletin de la Societe de chimie biologique* **1962**, *44*, 171-83.
62. Seddon, J. M.; Kaye, R. D.; Marsh, D., Induction of the Lamellar-Inverted Hexagonal Phase Transition in Cardiolipin by Protons and Monovalent Cations. *Biochimica et Biophysica Acta (BBA) - Biomembranes* **1983**, *734*, 347-352.
63. Olofsson, G.; Sparr, E., Ionization Constants Pka of Cardiolipin. *PLOS ONE* **2013**, *8*, e73040.
64. Gomez, B., Jr.; Robinson, N. C., Quantitative Determination of Cardiolipin in Mitochondrial Electron Transferring Complexes by Silicic Acid High-Performance Liquid Chromatography. *Analytical biochemistry* **1999**, *267*, 212-6.
65. Ott, M.; Robertson, J. D.; Gogvadze, V.; Zhivotovsky, B.; Orrenius, S., Cytochrome C Release from Mitochondria Proceeds by a Two-Step Process. *Proceedings of the National Academy of Sciences* **2002**, *99*, 1259-1263.
66. Orrenius, S.; Zhivotovsky, B., Cardiolipin Oxidation Sets Cytochrome C Free. *Nat Chem Biol* **2005**, *1*, 188-189.
67. Kapralov, A. A., et al., The Hierarchy of Structural Transitions Induced in Cytochrome C by Anionic Phospholipids Determines Its Peroxidase Activation and Selective Peroxidation During Apoptosis in Cells. *Biochemistry* **2007**, *46*, 14232-44.
68. Kagan, V. E., et al., Cytochrome C Acts as a Cardiolipin Oxygenase Required for Release of Proapoptotic Factors. *Nat Chem Biol* **2005**, *1*, 223-232.
69. Belikova, N. A.; Vladimirov, Y. A.; Osipov, A. N.; Kapralov, A. A.; Tyurin, V. A.; Potapovich, M. V.; Basova, L. V.; Peterson, J.; Kurnikov, I. V.; Kagan, V. E., Peroxidase Activity and Structural Transitions of Cytochrome C Bound to Cardiolipin-Containing Membranes. *Biochemistry* **2006**, *45*, 4998-5009.
70. Mabrouk, P. A.; Spiro, T. G., New Insights into Horseradish Peroxidase Function in Benzene from Resonance Raman Spectroscopy. *Journal of the American Chemical Society* **1998**, *120*, 10303-10309.
71. Everse, J.; Grisham, M. B.; Everse, K. E., *Peroxidases in Chemistry and Biology*; Taylor & Francis, 1990.
72. Grisham, M. B., Myoglobin-Catalyzed Hydrogen Peroxide Dependent Arachidonic Acid Peroxidation. *Journal of free radicals in biology & medicine* **1985**, *1*, 227-32.
73. Matsui, T.; Ozaki, S.-i.; Watanabe, Y., On the Formation and Reactivity of Compound I of the His-64 Myoglobin Mutants. *Journal of Biological Chemistry* **1997**, *272*, 32735-32738.
74. McClelland, L. J.; Mou, T.-C.; Jeakins-Cooley, M. E.; Sprang, S. R.; Bowler, B. E., Structure of a Mitochondrial Cytochrome C Conformer Competent for Peroxidase Activity. *Proc. Nat. Acad. Sci. USA* **2014**, *111*, 6648-6653.
75. Hanske, J.; Toffey, J. R.; Morenz, A. M.; Bonilla, A. J.; Schiavoni, K. H.; Pletneva, E. V., Conformational Properties of Cardiolipin-Bound Cytochrome C. *Proceedings of the National Academy of Sciences of the United States of America* **2012**, *109*, 125-30.
76. Spiro, T. G.; Strekas, T. C., Resonance Raman Spectra of Hemoglobin and Cytochrome C: Inverse Polarization and Vibronic Scattering. *Proceedings of the National Academy of Sciences* **1972**, *69*, 2622-2626.
77. Wright, P. G.; Stein, P.; Burke, J. M.; Spiro, T. G., Resonance Raman Spectra, Excitation Profiles and Excited (Iron .Fwdarw. Pyridine Charge Transfer) State Geometry of Bispyridine Iron(Ii) Heme. *Journal of the American Chemical Society* **1979**, *101*, 3531-3535.
78. Burke, J. M.; Kincaid, J. R.; Peters, S.; Gagne, R. R.; Collman, J. P.; Spiro, T. G., Structure-Sensitive Resonance Raman Bands of Tetraphenyl and "Picket Fence" Porphyrin-Iron

Complexes, Including an Oxyhemoglobin Analog. *Journal of the American Chemical Society* **1978**, *100*, 6083-6088.
79. Stong, J. D.; Burke, J. M.; Daly, P.; Wright, P.; Spiro, T. G., Resonance Raman Spectra of Nitrosyl Heme Proteins and of Porphyrin Analogs. *Journal of the American Chemical Society* **1980**, *102*, 5815-5819.
80. Choi, S.; Spiro, T. G., Out-of-Plane Deformation Modes in the Resonance Raman Spectra of Metalloporphyrins and Heme Proteins. *Journal of the American Chemical Society* **1983**, *105*, 3683-3692.
81. Spiro, T. G.; Smulevich, G.; Su, C., Probing Protein Structure and Dynamics with Resonance Raman Spectroscopy: Cytochrome C Peroxidase and Hemoglobin. *Biochemistry* **1990**, *29*, 4497-4508.
82. Hu, S.; Morris, I. K.; Singh, J. P.; Smith, K. M.; Spiro, T. G., Complete Assignment of Cytochrome C Resonance Raman Spectra Via Enzymic Reconstitution with Isotopically Labeled Hemes. *Journal of the American Chemical Society* **1993**, *115*, 12446-12458.
83. Unger, E.; Dreybrodt, W.; Schweitzer-Stenner, R., Conformational Properties of Nickel(Ii) Meso-Tetraphenylporphyrin in Solution. Raman Dispersion Spectroscopy Reveals the Symmetry of Distortions for a Nonplanar Conformer. *The Journal of Physical Chemistry A* **1997**, *101*, 5997-6007.
84. Alessi, M.; Hagarman, A. M.; Soffer, J. B.; Schweitzer-Stenner, R., In-Plane Deformations of the Heme Group in Native and Nonnative Oxidized Cytochrome C Probed by Resonance Raman Dispersion Spectroscopy. *Journal of Raman Spectroscopy* **2011**, *42*, 917-925.
85. Nie, S.; Emory, S. R., Probing Single Molecules and Single Nanoparticles by Surface-Enhanced Raman Scattering. *Science* **1997**, *275*, 1102-1106.
86. Hildebrandt, P.; Stockburger, M., Cytochrome C at Charged Interfaces. 1. Conformational and Redox Equilibria at the Electrode/Electrolyte Interface Probed by Surface-Enhanced Resonance Raman Spectroscopy. *Biochemistry* **1989**, *28*, 6710-21.
87. Hildebrandt, P.; Stockburger, M., Cytochrome C at Charged Interfaces. 2. Complexes with Negatively Charged Macromolecular Systems Studied by Resonance Raman Spectroscopy. *Biochemistry* **1989**, *28*, 6722-6728.
88. Murgida, D. H.; Hildebrandt, P., Heterogeneous Electron Transfer of Cytochrome C on Coated Silver Electrodes. Electric Field Effects on Structure and Redox Potential. *The Journal of Physical Chemistry B* **2001**, *105*, 1578-1586.
89. Murgida, D. H.; Hildebrandt, P., Electrostatic-Field Dependent Activation Energies Modulate Electron Transfer of Cytochrome C. *The Journal of Physical Chemistry B* **2002**, *106*, 12814-12819.
90. Murgida, D. H.; Hildebrandt, P.; Wei, J.; He, Y. F.; Liu, H.; Waldeck, D. H., Surface-Enhanced Resonance Raman Spectroscopic and Electrochemical Study of Cytochrome C Bound on Electrodes through Coordination with Pyridinyl-Terminated Self-Assembled Monolayers. *The Journal of Physical Chemistry B* **2004**, *108*, 2261-2269.
91. Hildebrandt, P.; Stockburger, M., Surface-Enhanced Resonance Raman Spectroscopy of Cytochrome C at Room and Low Temperatures. *The Journal of Physical Chemistry* **1986**, *90*, 6017-6024.
92. Hildebrandt, P.; Heimburg, T.; Marsh, D., Quantitative Conformational Analysis of Cytochrome C Bound to Phospholipid Vesicles Studied by Resonance Raman Spectroscopy. *European biophysics journal : EBJ* **1990**, *18*, 193-201.
93. Oellerich, S.; Lecomte, S.; Paternostre, M.; Heimburg, T.; Hildebrandt, P., Peripheral and Integral Binding of Cytochrome C to Phospholipids Vesicles. *J. Phys. Chem. B.* **2004**, *108*, 3781-3878.
94. Rytömaa, M.; Kinnunen, P. K., Evidence for Two Distinct Acidic Phospholipid-Binding Sites in Cytochrome C. *Journal of Biological Chemistry* **1994**, *269*, 1770-1774.

95. Rytōman, M.; Mustonen, P.; Kinnunen, P. K. J., Reversible, Nonionic and Ph-Dependent Association of Cytochrome C with Cardiolipin- Phosphatidylcholine Liposomes. *J. Biol. Chem.* **1992**, *267*, 22243-22248.
96. Rytömaa, M.; Kinnunen, P. K. J., Reversibility of the Binding of Cytochrome C to Liposomes: Implications for Lipid-Protein Interactions. *Journal of Biological Chemistry* **1995**, *270*, 3197-3202.
97. Kawai, C.; Prado, F. M.; Nunes, G. L. C.; Di Mascio, P.; Carmona-Ribeiro, A. M.; Nantes, I. L., Ph-Dependent Interaction of Cytochrome C with Mitochondrial Mimetic Membranes: The Role of an Array of Positively Charged Amino Acid Residues. *J. Biol. Chem.* **2005**, *280*, 34709-34717.
98. Soffer, J. B. The Folded, Partially Folded, Misfolded, and Unfolded Conformations of Cytochrome C Probed by Optical Spectroscopy. Drexel University, Philadelphia, PA, 2013.
99. Tuominen, E. K. J.; Zhu, K.; Wallace, C. J. A.; Clark-Lewis, I.; Craig, D. B.; Rytömaa, M.; Kinnunen, P. K. J., Atp Induces a Conformational Change in Lipid-Bound Cytochrome C. *Journal of Biological Chemistry* **2001**, *276*, 19356-19362.
100. Sinibaldi, F.; Fiorucci, L.; Patriacra, A.; Lauceri, R.; Ferri, T.; Cletta, M.; Santucci, R., Insights into Cytochrome C - Cardiolipin Interaction. Role Played by Ionic Strength. *Biochemistry* **2008**, *47*, 6928-6935.
101. Tuominen, E. K.; Wallace, C. J.; Kinnunen, P. K., Phospholipid-Cytochrome C Interaction: Evidence for the Extended Lipid Anchorage. *The Journal of biological chemistry* **2002**, *277*, 8822-6.
102. Kalanxhi, E.; Wallace, C. J. A., Cytochrome C Impaled: Investigation of the Extended Lipid Anchorage of a Soluble Protein to Mitochondrial Membrane Models. . *Biochem J.* **2007**, *407*, 179-187.
103. Kostrzewa, A.; Páli, T.; Froncisz, W.; Marsh, D., Membrane Location of Spin-Labeled Cytochrome C Determined by Paramagnetic Relaxation Agents. *Biochemistry* **2000**, *39*, 6066-6074.
104. Balakrishnan, g.; Hu, y.; Spiro, T. G., H26 Protonation in Cytochrome C Triggers Microsecond B-Sheet Formation and Heme Exposure: Implications for Apoptosis. *J. Am. Chem. Soc.* **2012**, *134*, 19061-19069.
105. Muenzner, J.; Toffey, J. R.; Hong, Y.; Pletneva, E. V., Becoming a Peroxidase: Cardiolipin-Induced Unfolding of Cytochrome C. *J Phys Chem B* **2013**, *117*, 12878-12886.
106. Hong, Y.; Muenzner, J.; Grimm, S. K.; Pletneva, E. V., Origin of the Conformational Heterogeneity of Cardiolipin-Bound Cytochrome C. *J. Am. Chem. Soc.* **2012**, *134*, 18713-18723.
107. Pandiscia, L. A.; Schweitzer-Stenner, R., Coexistence of Native-Like and Non-Native Cytochrome C on Anionic Liposomes with Different Cardiolipin Content. *The Journal of Physical Chemistry B* **2015**, *119*, 12846-12859.
108. Long, D. A., Classical Theory of Rayleigh and Raman Scattering. In *The Raman Effect*, John Wiley & Sons, Ltd: 2002; pp 31-48.
109. Long, D. A., Quantum Mechanical Theory of Rayleigh and Raman Scattering. In *The Raman Effect*, John Wiley & Sons, Ltd: 2002; pp 49-84.
110. Long, D. A., Vibrational Resonance Raman Scattering. In *The Raman Effect*, John Wiley & Sons, Ltd: 2002; pp 221-270.
111. Shelnutt, J. A.; O'Shea, D. C., Resonance Raman Spectra of Copper Tetraphenylporphyrin: Effects of Strong Vibronic Coupling on Excitation Profiles and the Absorption Spectrum. *The Journal of Chemical Physics* **1978**, *69*, 5361-5374.
112. Schweitzer-Stenner, R.; Stichternath, A.; Dreybrodt, W.; Jentzen, W.; Song, X.-Z.; Shelnutt, J. A.; Nielsen, O. F.; Medforth, C. J.; Smith, K. M., Raman Dispersion Spectroscopy on the Highly Saddled Nickel(Ii)-Octaethyltetraphenylporphyrin Reveals the Symmetry of

Nonplanar Distortions and the Vibronic Coupling Strength of Normal Modes. *The Journal of Chemical Physics* **1997**, *107*, 1794-1815.
113. Shelnutt, J. A., Normal-Coordinate Structural Decomposition and the Vibronic Spectra of Porphyrins. *Journal of Porphyrins and Phthalocyanines* **2001**, *5*, 300-311.
114. Hübner, W.; Mantsch, H. H.; Kates, M., Intramolecular Hydrogen Bonding in Cardiolipin. *Biochimica et Biophysica Acta (BBA) - Biomembranes* **1991**, *1066*, 166-174.
115. Malyshka, D.; Pandiscia, L. A.; Schweitzer-Stenner, R., Cardiolipin Containing Liposomes Are Fully Ionized at Physiological Ph. An Ft-Ir Study of Phosphate Group Ionization. *Vibrational Spectroscopy* **2014**, *75*, 86-92.
116. Malyshka, D.; Schweitzer-Stenner, R., Ferrocyanide-Mediated Photoreduction of Ferricytochrome C Utilized to Selectively Probe Non-Native Conformations Induced by Binding to Cardiolipin-Containing Liposomes. *Chemistry – A European Journal* **2017**, *23*, 1151-1156.
117. Milorey, B.; Malyshka, D.; Schweitzer-Stenner, R., Ph Dependence of Ferricytochrome C Conformational Transitions During Binding to Cardiolipin Membranes: Evidence for Histidine as the Distal Ligand at Neutral Ph. *The Journal of Physical Chemistry Letters* **2017**, *8*, 1993-1998.
119. Sathappa, M.; Alder, N. N., The Ionization Properties of Cardiolipin and Its Variants in Model Bilayers. *Biochimica et biophysica acta* **2016**, *1858*, 1362-72.